THE PLANT CELL

The Plant Cell, 2025, **37**, koae252

https://doi.org/10.1093/plcell/koae252
Advance access publication 7 October 2024
Research Article

Metabolic modeling reveals distinct roles of sugars and carboxylic acids in stomatal opening as well as unexpected carbon fluxes

Noah Sprent,[1] C.Y. Maurice Cheung,[2] Sanu Shameer,[3] R. George Ratcliffe,[4] Lee J. Sweetlove,[4] Nadine Töpfer[2,*]

[1]Department of Chemical Engineering, Imperial College London, South Kensington Campus, Exhibition Road, London SW7 2AZ, UK
[2]Institute for Plant Sciences, University of Cologne, Zülpicher Str. 47b, 50674 Cologne, Germany
[3]School of Biology, Indian Institute of Science Education and Research Thiruvananthapuram, Maruthamala PO, Vithura, Thiruvananthapuram 695551, Kerala, India
[4]Department of Biology, University of Oxford, South Parks Road, Oxford OX1 3RB, UK
*Author for correspondence: ntoepfer@uni-koeln.de
The author responsible for distribution of materials integral to the findings presented in this article in accordance with the policy described in the Instructions for Authors (https://academic.oup.com/plcell/pages/General-Instructions) is: Nadine Töpfer (ntoepfer@uni-koeln.de).

Abstract

Guard cell metabolism is crucial for stomatal dynamics, but a full understanding of its role is hampered by experimental limitations and the flexible nature of the metabolic network. To tackle this challenge, we constructed a time-resolved stoichiometric model of guard cell metabolism that accounts for energy and osmolyte requirements and which is integrated with the mesophyll. The model resolved distinct roles for starch, sugars, and malate in guard cell metabolism and revealed several unexpected flux patterns in central metabolism. During blue light-mediated stomatal opening, starch breakdown was the most efficient way to generate osmolytes with downregulation of glycolysis allowing starch-derived glucose to accumulate as a cytosolic osmolyte. Maltose could also accumulate as a cytosolic osmoticum, although this made the metabolic system marginally less efficient. The metabolic energy for stomatal opening was predicted to be derived independently of starch, using nocturnally accumulated citrate which was metabolized in the tricarboxylic acid cycle to malate to provide mitochondrial reducing power for ATP synthesis. In white light-mediated stomatal opening, malate transferred reducing equivalents from guard cell photosynthesis to mitochondria for ATP production. Depending on the capacity for guard cell photosynthesis, glycolysis showed little flux during the day but was crucial for energy metabolism at night. In summary, our analyses have corroborated recent findings in Arabidopsis guard cell research, resolved conflicting observations by highlighting the flexibility of guard cell metabolism, and proposed new metabolic flux modes for further experimental testing.

Introduction

Regulated changes in stomatal aperture allow plants to balance the tradeoff between CO_2 uptake for photosynthesis and water loss by transpiration (Engineer et al. 2016; Zhang et al. 2018; Lawson and Vialet-Chabrand 2019). Signaling systems within the leaf provide information about carbon demand and water status, and this information is integrated to regulate guard cell volume and hence stomatal aperture (Assmann and Jegla 2016; Woolfenden et al. 2018). To increase guard cell volume and thereby increase stomatal aperture, the concentration of osmolytes within the guard cell must increase. Osmolytes can be taken up from the surrounding apoplast or generated within the guard cell by degradation of non-osmotic storage compounds such as starch. Despite a long research history, many aspects of osmoregulated stomatal opening remain unresolved (Lawson and Matthews 2020).

Early explanations for guard cell osmoregulation proposed that sucrose derived from guard cell starch degradation was the main guard cell osmolyte during stomatal opening (Lloyd 1908; Scarth 1927). This starch-sugar hypothesis held sway until the 1960s but subsequently fell out of favor due to a poor association between the amount of guard cell starch and stomatal aperture (Lawson and Matthews 2020) and the emergence of the K^+-malate hypothesis whereby stomatal opening is driven by uptake of K^+ from the apoplast and the counterions malate and/or Cl^- (Schnabl and Raschke 1980; Outlaw 1983). The latter has been the dominant paradigm for guard cell osmoregulation for the last few decades. However, quantitative analyses in Asiatic dayflower (*Commelina communis*) demonstrated that K^+ and its counterions did not provide a sufficient concentration of osmolytes to account for observed aperture changes in that species (MacRobbie and Lettau 1980), leading to a re-examination of the role of sugars as osmolytes. An integration of the starch-sugar and K^+-malate hypotheses was achieved with the proposal that K^+ is the main osmolyte for stomatal opening early in the day and sucrose becomes a substantial osmolyte later in the day to maintain stomatal aperture (Amodeo et al. 1996; Talbott and Zeiger 1996). More recently, the role of sucrose as an osmolyte in stomatal opening has been questioned in the light of evidence that its role is primarily energetic (Medeiros et al. 2018). Although it is becoming increasingly apparent that guard cell metabolism is an important contributor to stomatal dynamics

Received June 28, 2024. Accepted August 12, 2024

(Blatt 2016; Santelia and Lunn 2017), a clear picture of the role of guard cell metabolism is proving elusive (see also Lemonnier and Lawson (2024) for a recent extensive review on this topic).

Central to the debate is the combined potential for guard cell metabolites to act both as osmolytes and as a source of energy to drive osmolyte uptake and intracellular transport. Irrespective of whether osmolytes are generated within the guard cell or taken up from the surrounding apoplast, energy-dependent transport across membranes is required (Jezek and Blatt 2017). The majority of osmolytes must accumulate in the vacuole as this makes up the bulk of the guard cell volume. Transport of metabolites from the cytosol to the vacuole requires energization of the tonoplast by ATP- or PP_i-dependent proton pumps (Eisenach and De Angeli 2017). Additionally, energization of the plasma membrane by the H^+-ATPase causes hyperpolarization and activation of voltage-gated K^+-channels with uptake of further osmolytes including Cl^-, malate, and sugars from the apoplast (Assmann et al. 1985; Kinoshita et al. 2001; Kwak et al. 2001; Inoue and Kinoshita 2017; Jezek and Blatt 2017).

There are 3 ways in which the guard cell can potentially meet this energy requirement: via photosynthesis within guard cell chloroplasts; via respiration using respiratory substrates such as starch, sugars, or lipids generated by metabolism within the guard cell; or via respiration using sugars imported from the apoplast, and ultimately derived from the mesophyll. Based on the numbers of guard cell chloroplasts and mitochondria and measurements of their metabolic capacity, the prevailing view is that guard cells have limited photosynthetic capacity and that the bulk of the energy required for stomatal opening is met by respiration (Outlaw 1989; Reckmann et al. 1990; McLachlan et al. 2016; Lim et al. 2022). Furthermore, it has generally been considered that the limited amount of starch in guard cell chloroplasts means that the bulk of the substrate for respiration is provided by uptake of sugars and/or malate from the apoplast (Vavasseur and Raghavendra 2005; Lawson and Matthews 2020). Consistent with this, guard cell-specific over-expression of a gene encoding sucrose synthase led to reduced guard cell sucrose content during opening, while stomatal aperture increased, suggesting an energetic rather than osmotic role for guard cell sucrose (Daloso et al. 2015, 2016a, 2016b). This was corroborated by ^{13}C-labeling experiments with epidermal fragments in which ^{13}C from exogenous sugars appeared in TCA cycle carboxylic acids and related metabolites such as glutamine, suggesting that at least some of the imported sucrose was catabolized via respiration (Medeiros et al. 2018; Daubermann et al. 2024). However, the picture has been complicated by the discovery that breakdown of guard cell starch is required for normal stomatal opening triggered by blue light (Horrer et al. 2016). While earlier studies suggested that starch might provide additional respiratory substrates and/or osmolytes during the initial opening of the stomata at dawn (Blatt 2016), more recent findings suggest that rapid starch degradation at dawn is likely required to maintain sugar homeostasis during stomatal opening and to facilitate fast stomatal opening (Flütsch et al. 2020).

The analysis of guard cell starch-breakdown mutants has shed some light on the role of starch in blue light stomatal opening but has also raised questions (Flütsch et al. 2020). The main metabolic difference in the mutant lines during blue light stomatal opening was a pronounced decline in glucose levels. While this analysis suggests that the fate of mobilized starch is to support glucose homeostasis not malate synthesis, it remains unclear what the fate of the glucose is. Evidence was provided that the lack of glucose homeostasis affects stomatal dynamics and kinetics; but normal transport rates of H^+, K^+ and Cl^- in the starch mutants led the authors to conclude that starch-derived glucose was not acting as a respiratory substrate (Flütsch et al. 2020). However, the decline of glucose levels in epidermal peels of the starch-breakdown mutants when exposed to blue light also led the authors to conclude that the glucose is used as a respiratory substrate. This conclusion effectively assumes that the guard cell distinguishes between glucose derived from starch and glucose stores in the guard cell built up during the previous day which is difficult to envisage from a mechanistic perspective.

This mutant study highlights some of the problems with the experimental evidence that has been used to infer the contribution of guard cell metabolism to osmoregulation and energetics. First, metabolic activity—i.e. metabolic flux—needs to be quantified in addition to the levels of metabolites. When a metabolite level goes up, for example, it is not possible to tell without analysis of fluxes whether this is due to an increased influx into the pool, a reduced efflux from the pool, or some combination of both (Kruger and Ratcliffe 2009). Moreover, the analysis of the starch-breakdown mutants was based on single time point measurements (Flütsch et al. 2020). Given the highly dynamic nature of stomatal opening and the fact that other products of starch turnover such as maltose were not measured, the conclusions regarding glucose as a major starch-derived metabolite should be taken with caution and examined in further experimental work. Second, a quantitative accounting of energy supply and demand, alongside the metabolic contribution to osmoregulation is required to resolve the role of metabolism in guard cells. In practice, this is very difficult to achieve experimentally as it would require quantification of all the relevant transport fluxes (including those at both the tonoplast and the plasma membrane) as well as a detailed analysis of fluxes of energy metabolism within the guard cell (photosynthesis and respiration) and the rates of change of all relevant osmolytes. Moreover, all this information would need to be collected in the same experimental system as the experimental conditions, and in particular the availability of ions and metabolites external to the guard cell, are likely to strongly affect the outcome. In reality, most of the available data is incomplete (e.g. measurement of some transport fluxes but not others) and combines different experimental systems (e.g. isolated guard cells, epidermal peels, and whole leaf measurements). Finally, while the use of guard cell-specific mutants can be informative, compensatory metabolic changes in the mutant may mislead as to the situation in the WT. Thus, currently there is no comprehensive data set of metabolic fluxes and direct measures of energy fluxes at the guard cell level available.

Computational modeling, on the other hand, can provide an integrated analysis of all relevant metabolic and transport fluxes and there is a long history of modeling stomatal dynamics (Blatt et al. 2022). Several models have focused on empirical capture of the regulatory responses to water availability and CO_2 demand (Sperry et al. 2017) or on the mechanisms of osmolyte transport (Chen et al. 2012). The OnGuard framework (Hills et al. 2012) allows quantitative dynamic modeling of guard cell behavior by simulating transporters at the plasma membrane and tonoplast. The most recent iteration, OnGuard3, models the interplay of foliar CO_2 diffusion and mesophyll photosynthesis, and thus connects transport processes at the guard cell membrane to gas exchange of the whole plant (Jezek et al. 2021). Despite these advances in modeling stomatal physiology, there are relatively few models that consider guard cell metabolism and its role in stomatal movement.

An important first step in addressing this gap was the construction and analysis of a flux-balance model of guard cell metabolism

(Robaina-Estévez et al. 2017) based on a model of primary metabolism in Arabidopsis (*Arabidopsis thaliana*) (Arnold and Nikoloski 2014). In this framework, metabolic fluxes were estimated by maximizing their concordance with cell-type-specific transcriptome data for guard and mesophyll cells. The analysis predicted that guard cell photosynthesis and carbon fixation in the chloroplast were active, leading to starch and sucrose biosynthesis. Additionally, the model predicted that malate decarboxylation in the chloroplast was the main source of CO_2 for carbon fixation by Rubisco, similar to C_4 and CAM photosynthesis albeit without the spatial and temporal separation. While this model demonstrated the potential of constraint-based modeling in the context of guard cell metabolism, it has several limitations. First, it relies on flux solutions that match transcript abundances of the respective enzymes even though it is well established that there is no simple relationship between transcript abundance and flux (Schwender et al. 2014). Second, it represents a single metabolic steady-state and can therefore say nothing about stomatal dynamics. Third, it lacks an explicit representation of the accumulation of osmolytes and therefore does not account for the cost of osmolyte transport during guard cell volume changes. Finally, it makes separate comparisons of mesophyll and guard cell metabolism even though it is known that their metabolism is interconnected (Lawson et al. 2014).

Some of these shortcomings were addressed in a multiphase flux-balance model of guard cell metabolism (Tan and Cheung 2020). Guard cell metabolism was modeled over 4 distinct phases of the diel cycle representing day and night and stomatal opening and closing. Guard cell-specific metabolism was modeled by simulating the accumulation of osmolytes during the opening and day phases. To model the contribution of the mesophyll to osmotic requirements for stomatal opening, a fixed value of sucrose import from the apoplast was set. The model predicted an alternative flux mode of the Calvin–Benson–Bassham cycle during stomatal opening which maximized pyrophosphate (PP_i) production to drive the pumping of protons across the tonoplast and to enable subsequent accumulation of osmolytes in the vacuole during stomatal opening. An analysis of the energetics in the model found that malate and Cl^- were similarly efficient as the counterion for K^+ during stomatal opening. A drawback of this study was that the model behavior was mainly dictated by constraints based on known behavior of guard cell metabolites and osmolytes. For instance, the model was only allowed to use K^+, Cl^-, malate, and sucrose as osmolytes, and starch and sucrose as carbon and energy reserves. While this model incorporated some important aspects of guard cell metabolism such as the temporal changes in osmolyte levels and the associated cost of osmolyte transport, it failed to answer relevant questions due to the nature of its constraints. For instance, it cannot resolve the role of glucose as metabolite and osmolyte during stomatal opening (Flütsch et al. 2020), or the contribution of guard cell photosynthesis and of the mesophyll to the overall leaf energetics.

Here, we report a more advanced flux-balance model that integrates guard cell and mesophyll metabolism. By representing several successive time intervals during the diel cycle, our model accounts for the metabolic, osmotic, and energetic changes as guard cells swell and shrink in volume during stomatal dynamics. To do this, we utilized the GrOE-FBA framework to predict (rather than constrain) the use of different osmolytes (Shameer et al. 2020); and we used experimentally determined stomatal aperture as an input to the model. We report the most efficient flux distributions in guard cells during stomatal opening in blue or white light by optimizing the model for overall photosynthetic productivity in the leaf. The results of this minimally constrained stoichiometric model provide a detailed quantitative accounting of guard cell energetics and osmolyte accumulation, and present a comprehensive picture of possible metabolic states of guard cells.

Results

Construction of an integrated stoichiometric model of guard cell and mesophyll metabolism with 4 temporal phases

The starting point for the integrated model was an earlier diel stoichiometric model of plant leaf metabolism, PlantCoreMetabolism_v1_2 (Shameer et al. 2018, 2020). The model consists of a detailed catalogue of all the subcellular reactions and transport steps required for autotrophic growth and has been extensively curated to ensure that the reactions of primary metabolism, the mechanisms and proton coupling of metabolite and ion transporters, and the effect of sub-compartmental pH on the ionic speciation state of carboxylates and phosphates are all accurately represented. Starting from this base model, our model reconstruction process involved the following steps.

First, to capture metabolic interactions between guard cells and the mesophyll, we duplicated the model to represent a guard cell and mesophyll cell connected by an apoplastic compartment with which both cells can exchange metabolites and ions, including protons (Fig. 1, see Materials and methods, Supplementary Fig. S1). We then added reactions to the guard cell model to account for known guard cell plasma membrane and tonoplast transporters and channels (see Materials and methods, Supplementary Fig. S2). To account for any difference in photosynthetic capacity between the mesophyll and guard cell, we derived equations which relate the total volume of guard cell and mesophyll and the capacity and number of chloroplasts in each cell type to the level of photon influx in each cell type (see Materials and methods).

Second, to represent stomatal aperture dynamics and to account for the energetics of the entire diel cycle, we quadrupled the 2 cell-type model, representing 4 distinct phases—Opening, Day, Night 1, and Night 2 (Fig. 1, see Materials and methods). Four phases are necessary to allow for the essence of diel stomatal dynamics to be captured. Day 1 and Day 2 represent stomatal opening and closing, and Night 1 and Night 2 allow capturing the diel pattern of starch levels (Horrer et al. 2016). To model the accumulation and degradation/export of metabolites and ions, these 4 phases were coupled by "linker" reactions that can transfer metabolites between adjacent time phases. For the mesophyll cell, we added the same linker reactions as used previously: sucrose, malate, citrate, and amino acids in the vacuole and starch in the plastid (Cheung et al. 2014). For the guard cell, we also added sucrose, $malate^{2-}$, $citrate^{3-}$, maltose, and palmitate linker reactions in the cytosol, and added K^+, Cl^-, NO_3^-, glucose, and fructose linker reactions in the vacuole and cytosol. The fatty acid palmitate was introduced as a linker metabolite to allow the utilization of lipids for the production of respiratory substrates during stomatal opening (McLachlan et al. 2016; Geilfus et al. 2018; Korte et al. 2023). We also added transport reactions for the osmolytes to the apoplast, except for citrate and the amino acids, where there has been no indication that these are exported/imported to/from the apoplast (see Supplementary Table S1). The model was constrained in a way that metabolites that accumulate in 1 or more phases will be consumed in subsequent phases in order to close the diel loop. For example, starch levels at the beginning of Night 2 must match those at the end of Night 1.

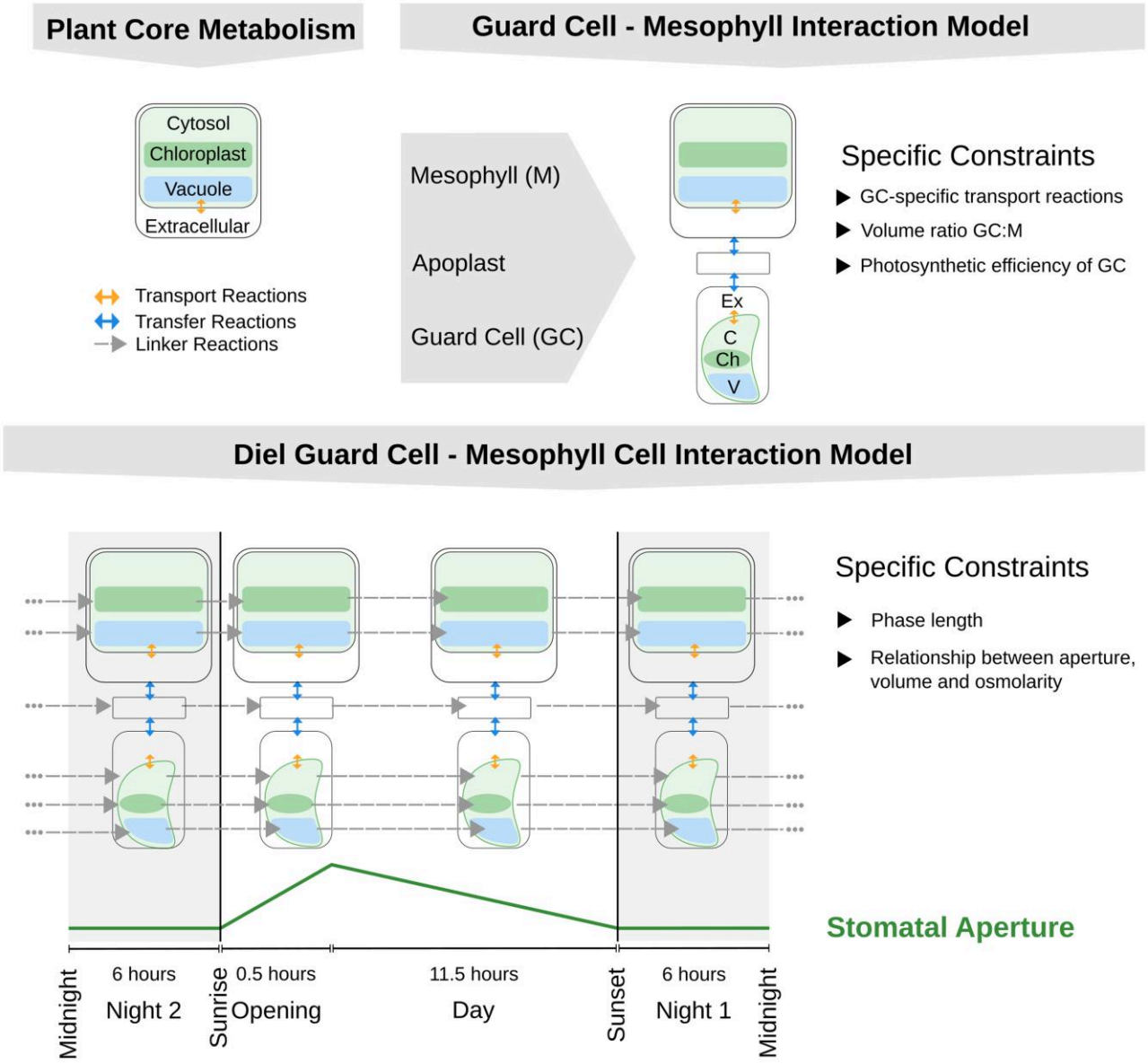

Figure 1. Construction of an integrated model of guard cell and mesophyll cell metabolism. Top left: Starting point for the model construction was a stoichiometric core model of cellular metabolism which accounts for plant primary metabolism and subcellular compartmentation (Shameer et al. 2018). For clarity only chloroplast, cytosol and vacuole are shown. "Transport" reactions move ions/metabolites between compartments within the cell, "transfer" reactions connect the cell to an apoplast compartment, and "linker" reactions can move ions/metabolites from 1 phase to the next thus allowing the simulation of accumulation and degradation patterns. Top right: To create a combined model of guard cell and mesophyll cell metabolism, this core model was replicated, guard cell-specific transport reactions and photosynthetic efficiency assumptions were added to the guard cell model, and the cell volumes were constrained relative to one another. Bottom: Finally, this combined model was replicated to create 4 temporal phases capturing the main phases of guard cell metabolism accounting for environment and species-specific constraints such as light quality and intensity, aperture, volume, and osmolarity changes during stomatal opening and closing at the beginning of the day. Linker reaction arrows with a dotted line represent ion/metabolite movements that link the end and beginning of the diel cycle. This generic guard cell–mesophyll interaction model was then constrained by specified metabolic and osmotic constraints and simulated to optimize overall photosynthetic productivity in the leaf. Modeling predictions are optimal osmolyte concentrations and metabolic fluxes.

Third, we modeled changes in the turgor pressure of the guard cells which drive the changes in volume necessary to open and close stomata. To provide a way to constrain the turgor pressure, we used the GrOE-FBA framework (Shameer et al. 2020). This framework constrains the total osmolyte concentration in the cell to a specified value, but leaves unconstrained which metabolites and ions are accumulated. In our model, we incorporated equations from the OnGuard model (Hills et al. 2012) to calculate the osmolarity and volume of the guard cells required for specific stomatal apertures. Thus, we can specify the aperture of the stomata at the end of each phase based on information from the literature. This in turn constrains the model to accumulate the right amount of osmoticum for that given aperture. See Materials and methods for details of all calculations.

Overall, this metabolic modeling framework represents a generic guard cell—mesophyll cell system which can be parameterized according to the system under consideration. To arrive at a context-specific representation, we can specify the light intensity (PPFD) of the light source illuminating the leaf, the aperture of the stomata, the length of each phase, and the anatomical

Table 1. Environmental and Arabidopsis-specific parameters used to constrain the model

Parameter	Description	Value	Units	Source
PPFD	Photosynthetic Photon flux density	150	$\mu mol \cdot m^{-2} \cdot s^{-1}$	(Horrer et al. 2016)
P_{abs}	Proportion of light absorbed by leaf	0.9	Dimensionless	(Zhu et al. 2010)
T_L	Thickness of leaf	1.7×10^{-4}	m	(Wuyts et al. 2010)
V_{gcind}	Volume of individual GC	4.75×10^{-13}	dm^3	(Jezek and Blatt 2017)
F_qF_m	PS efficiency of GC as proportion of MC	0.9	Dimensionless	(Lawson et al. 2003)
R_{ch}	Ratio of chloroplast number GC:MC	0.0692	Dimensionless	(Fujiwara et al. 2019)
R_{chvol}	Ratio of chloroplast volume GC:MC	0.2005	Dimensionless	(Knoblauch et al. 2023)
$Prop_{air}$	Proportion of leaf that is air	0.37	Dimensionless	(Earles et al. 2018)
$Prop_{epidermis}$	Proportion of leaf that is epidermis	0.15	Dimensionless	(Wuyts et al. 2010)
Vacfrac	Proportion of GC that is vacuole	0.751	Dimensionless	(Wang et al. 2017)
T	Temperature	296.15	K	(Horrer et al. 2016)
N_{gcs}	Number of GCs in model	5.8 × 108	m^{-2}	(Papanatsiou et al. 2017)
n	Osmolarity parameter	2.5	atm	(Wang et al. 2017)
m	Osmolarity parameter	0.8	$atm \cdot \mu m^{-1}$	(Wang et al. 2017)
r	Osmolarity parameter	5×10^{-14}	$dm^3 \cdot \mu m^{-1}$	(Wang et al. 2017)
s	Osmolarity parameter	3×10^{-13}	dm^3	(Wang et al. 2017)
C_{apo}	Osmolarity of the apoplast	0.0230	$mol \cdot dm^{-3}$	(Wang et al. 2017)
Aclosed	Closed aperture	1.6	µm	(Horrer et al. 2016)
Aopen	Open aperture	2.75	µm	(Horrer et al. 2016)
H+-ATPase	Plasma membrane H+-ATPase constraint	7.5	$fmol \cdot h^{-1}$	(Jezek et al. 2021)

Parameter values used to predict osmolyte levels and metabolic fluxes in guard and mesophyll cells in an Arabidopsis leaf were collected from the corresponding source. *n*, *m*, *r*, and *s* are empirical parameters used in the OnGuard model for calculating guard cell osmolarity (see Materials and methods).
GC, guard cell; MC, mesophyll cell; PS, photosynthetic.

parameters of our system of interest which are then converted into constraints in the model. Additionally, the number and length of the phases can also be adjusted to model a different system. The model can be solved as a single optimization problem that fulfills the given constraints and predicts flux patterns and osmolyte levels that maximize the export of sucrose and amino acids at a defined composition from the mesophyll to the phloem (phloem output) over the diel cycle (see Materials and methods, Supplementary Data Set 1).

Table 1 lists the parameters from *A. thaliana* which were used in the model. We based the duration of the 4 phases on the pattern of stomatal aperture reported for *A. thaliana*, with a half-hour opening phase, 11.5 h day phase, and two 6 h night phases (Horrer et al. 2016) and scaled the linker reactions appropriately to adjust for the differences in length (see Materials and methods). Additionally, we used a closed aperture of 1.6 µm, an open aperture of 2.75 µm, and a PPFD of 150 $\mu mol \cdot m^{-2} \cdot s^{-1}$ as reported in the same study. As experimentally determined starch levels in our reference study were of semi-quantitative nature (starch granule area), we did not add any constraints on starch levels to the model (Horrer et al. 2016). Using these parameters, osmolarity increased by ~37 mM during opening, from 179 mM to 216 mM, which was similar to the measured increase in concentration of 47 mM (Flütsch et al. 2020). Per guard cell, this corresponded to an increase of 27 fmol, from 68 fmol to 95 fmol.

Leaf maintenance costs were calculated based on a previous derived light-dependent equation (Töpfer et al. 2020). To calculate the relative contributions of maintenance from mesophyll and guard cells, we derived a proxy for the relative metabolic activities for mesophyll and guard cells based on the sum of absolute metabolic fluxes. The calculated maintenance costs were used to constrain ATP and NADPH-consuming maintenance reactions in the model (see Materials and methods).

The model was solved using parsimonious FBA (pFBA), first optimizing the main objective, in this case phloem output from the leaf, before minimizing the sum of absolute fluxes in the model. This minimization of fluxes assumes that metabolism has evolved to be efficient in its use of enzymes, and it also avoids potential artifacts such as futile cycles in model solutions. Further details of this process can be found in the Materials and methods section.

We then used this species-specific integrated guard cell—mesophyll model to investigate optimal metabolic fluxes in *A. thaliana* guard and mesophyll cells under a range of physiologically relevant scenarios. After initial investigation without any additional kinetic constraints, we found that our model overestimated the guard cell plasma membrane H^+-ATPase flux with 14.0 fmol GC^{-1} h^{-1} as compared to 7.5 fmol GC^{-1} h^{-1} calculated from the OnGuard model (Hills et al. 2012). The import of K^+ and Cl^- was sufficient for stomatal opening with no starch accumulation over the diel cycle, suggesting that ion import is more efficient in providing osmoticum compared to starch degradation. To generate a realistic energy-bound for ion transport, we set an upper bound of 7.5 fmol GC^{-1} h^{-1} on the flux through the guard cell plasma membrane H^+-ATPase (Supplementary Fig. S3). We simulated both blue and white light stomatal opening which represents stomatal opening in the morning or during the day, respectively. Furthermore, to investigate the role of guard cell starch metabolism and the photosynthetic contribution of the guard cell to stomatal opening, we simulated both WT and guard cell starch-knockout metabolism as well as guards cells that lack any photosynthetic contribution. The values for all parameters and the sources for them can be found in Table 1. Although the model solution is a prediction of optimal fluxes over the entire diel cycle in both the guard cell and mesophyll cell, unless otherwise stated, we analyze and present only fluxes from the guard cell during the opening phase.

Distinct roles for starch and carboxylic acids in blue light stomatal opening

When stomata open at dawn, they do so in blue light that contains little photosynthetically active radiation. Experimental settings to study blue light opening typically use a fluence rate insufficient for the activation of guard cell photosynthesis. To resolve the metabolic flux states that allow guard cell expansion under these conditions, we prevented photosynthesis during the opening phase of the model (Fig. 1). As expected, import of K^+ and Cl^- ions into the guard cell from the apoplast made a substantial contribution (55%) to the increase in osmolarity during stomatal opening, with an increase of 30 mM (Fig. 2A, for full results in this section,

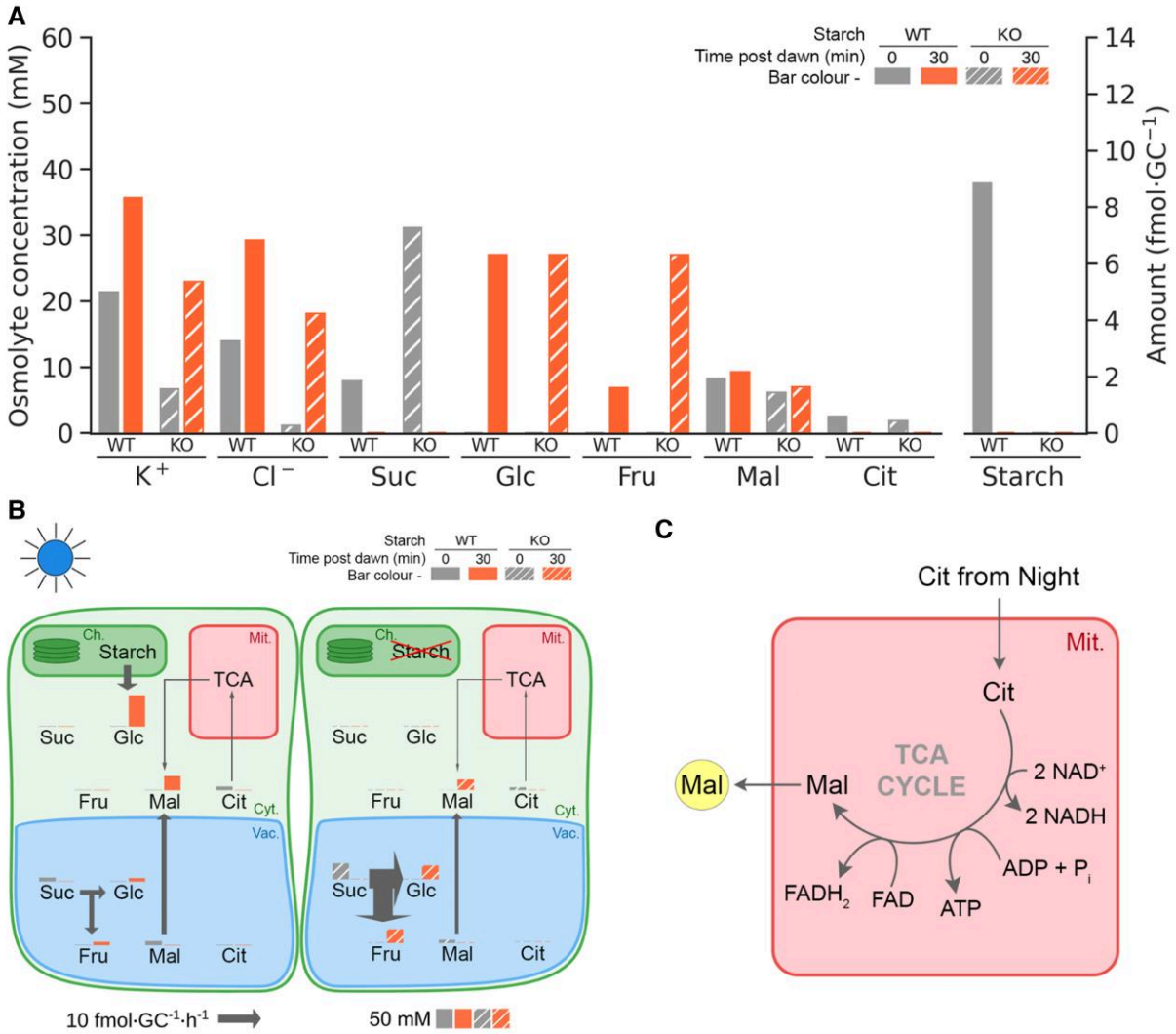

Figure 2. Osmolyte concentrations and metabolic fluxes in the guard cell during opening in blue light. **A)** Overall concentration of osmolytes and amount of starch per guard cell in WT and starch knockout mutant. **B)** Bars show compartment-specific concentrations of organic osmolytes and arrows show metabolic fluxes, with the width the arrows scaled linearly to flux. **C)** The flux mode for the partial TCA cycle that generates reducing power and ATP. Circled metabolites represent osmotica for stomatal opening. Ch., chloroplast; Cit, citrate; Cyt., cytosol; Fru, fructose; GC, guard cell; Glc, glucose; KO, knockout; Mal, malate; Mit., mitochondrion; Suc, sucrose; TCA, tricarboxylic acid cycle; Vac., vacuole; WT, wild type.

see Supplementary Data Set 2). Moreover, the model predicted the breakdown of guard cell starch during the opening phase (Fig. 2B), which is an important result that is consistent with experimental data showing that starch breakdown is required for blue light-stimulated stomatal opening (Flütsch et al. 2020).

The model also revealed the fate of the glucose produced by the starch degradation, allowing open questions about the role of starch breakdown in the supply of osmoticum and energy to be addressed. We found an unusual flux pattern in guard cell central metabolism that suggests that the fate of starch in blue light opening is exclusively to supply osmoticum in the cytosol and not to participate in energy metabolism. Starch was catabolized using the amylolytic pathway, which first breaks starch down into maltose which is then hydrolyzed to glucose. The model predicted that none of this starch-derived glucose was transported into the vacuole for osmoticum. Instead, the model used 2 energetically cheaper solutions in the vacuole: (i) importing K^+ and Cl^- ions into the vacuole (requiring 1 proton to be pumped into the vacuole) compared to importing 2 molecules of glucose (requiring 2 protons to be pumped into the vacuole); and (ii) breaking down sucrose by vacuolar invertase to form glucose and fructose in the vacuole. Surprisingly, none of the cytosolic glucose entered glycolysis and glycolytic flux was essentially absent during this phase of opening. This can be rationalized as a means of allowing cytosolic glucose derived from starch to accumulate, by restricting its onward metabolism via glycolysis. An alternative possibility is that other intermediates in the pathway of starch breakdown could accumulate instead of, or as well, as glucose. Indeed, rapid accumulation of maltotriose and maltose has been reported in a study of *Vicia faba* epidermal peels exposed to blue light (Talbott and Zeiger 1993). To test this possibility, we performed an additional simulation and found that maltose only accumulated in the model when cytosolic hexose accumulation was blocked. This makes sense at an osmotic level: Splitting 1 molecule of maltose into 2 molecules of glucose generates twice as much osmotic potential and hence is more efficient. However, the overall efficiency loss was marginal (0.00014%).

With starch and sugar making no contribution to energy metabolism in the guard cell, the question arises as to how stomatal opening is powered in blue light. In the model, the energy required

for opening was derived from the metabolism of a small amount of citrate (2.5 mM change in concentration) that had accumulated in the cytosol in the dark (Fig. 2A). Citrate was metabolized to malate through the TCA cycle providing reducing power for mitochondrial ATP synthesis (Fig. 2C). The resulting malate accumulated during the day and was reconverted to citrate at night, completing the citrate–malate cycle over the diel cycle. There was no gluconeogenic flux, so citrate made no contribution to sugar homeostasis and instead was exclusively used for energy metabolism.

To confirm the role of starch in providing osmoticum but not energy during blue light stomatal opening, we simulated a starch breakdown knockout mutant by adding a constraint to the model that prevented guard cell starch breakdown. In this scenario, although the model took up the same amount of K^+ and Cl^- from the apoplast as in the WT model, less was imported into the vacuole so that more could be retained in the cytosol to contribute to its osmotic potential in the absence of starch-derived cytosolic glucose. Note that the differences in the concentrations of K^+ and Cl^- between WT and starch knockout were due to the differences in the basal levels of K^+ and Cl^- in the guard cell at the end of the dark period, but the changes in K^+ and Cl^- concentration were the same (Fig. 2A). Part of the basal levels of K^+ and Cl^- was instead replaced by maltose, which from a computational perspective are equivalent as they have the same osmotic coefficient. To compensate for the reduced KCl content of the vacuole, the model accumulated close to 4 times more sucrose in the vacuole overnight than in WT and this was broken down during opening by vacuolar invertase to form glucose and fructose, providing an osmotic contribution of 54 mM (Fig. 2, A and B). Energy was still exclusively provided by the metabolism of citrate into malate via the TCA cycle.

In summary, these results suggest that the role of starch breakdown during blue light opening is to provide glucose for cytosolic osmoticum and that energy is supplied by the metabolism of citrate to malate with no contribution from glycolysis. In the model, this is the most efficient way of balancing the osmotic and energy requirements of stomatal opening. If starch breakdown is not possible, the next most efficient metabolic mode is to degrade vacuolar sucrose stored overnight into vacuolar hexoses and to retain more K^+ and Cl^- in the cytosol for osmoticum.

Sugars for osmoticum are provided by guard cell starch breakdown and photosynthesis in white light stomatal opening

In the blue light opening scenario, photon influx was prevented during the opening phase and permitted during the day according to the photosynthetic capacities of the guard cell and the mesophyll (see Materials and methods). To observe how photosynthesis might contribute to the osmotic and energy requirements during opening, we also simulated the model with photon influx into the guard cell and mesophyll during the opening phase. As before, we simulated both a WT and a starch degradation knockout scenario (Fig. 3; for full results, see Supplementary Data Set 2).

In the WT simulation, in the same way as in the blue light scenario, K^+ and Cl^- imported from the apoplast were the main source of osmolytes during stomatal opening, and starch was broken down to provide glucose that accumulated as osmoticum in the cytosol due to the absence of glycolytic flux (Fig. 3). Vacuolar sucrose was broken down to provide glucose and fructose as osmoticum in the vacuole. While the amount of starch broken down was 5.7% higher than in blue light, the amount of sucrose broken down was 22% lower. Guard cell photosynthesis played a minor role in the synthesis and accumulation of osmoticum in the cytosol (Fig. 3B). The amount of osmoticum produced from guard cell photosynthesis was 3% of that from starch degradation. Guard cell photosynthetic energy was sufficient for import of K^+ and Cl^- ions and for synthesis of sucrose from CO_2. However, to meet the demand for ATP in the cytosol (primarily due to the plasma membrane H^+-ATPase), a coordinated chloroplast-mitochondrion energy system was used. This involved shuttling of photosynthesis-generated reducing power (NADPH) via the malate-OAA metabolite shuttle to the mitochondrion (Fig. 3C). The NADH released in the mitochondrion due to mitochondrial malate dehydrogenase activity was used to fuel the mitochondrial electron transport chain and mitochondrial ATP synthase. Although the importance of mitochondrial metabolism to utilize chloroplast reducing power has been previously recognized (Shameer et al. 2019), the unusual feature of the metabolic flux mode predicted here was the use of mitochondrial electron transport in the absence of a TCA cycle flux, instead the electrons coming exclusively from malate shuttled from the chloroplast.

In white light, the model predicted the operation of an alternative flux mode of the Calvin–Benson–Bassham cycle that generated PP_i by using pyrophosphate: fructose-6-phosphate 1-phosphotransferase (PFP) and transaldolase instead of fructose-6-phosphatase and sedoheptulose-1,7-bisphosphatase in WT guard cells during stomatal opening. A similar flux mode was predicted in a previous modeling study, with the PP_i being used to fuel the tonoplast-pyrophosphatase (Tan and Cheung 2020). In contrast, the PP_i produced here was involved in a sucrose cycle that partially salvaged the Gibbs energy in PP_i while producing hexoses from sucrose as osmoticum (Fig. 3D). Instead of directly using invertase to break down sucrose into hexoses, the model predicted the use of sucrose synthase to produce UDP-glucose and fructose. Glucose-1-phosphate uridylyltransferase can combine PP_i and UDP-glucose to form glucose 1-phosphate and UTP, conserving the energy in PP_i (Fig. 3D). A cycle involving sucrose phosphate synthase, sucrose phosphatase, and sucrose synthase can then convert the resulting hexose phosphate into hexose for osmoticum. The net effect is the conversion of 1 sucrose into 2 fructose while combining 1 PP_i with 1 UDP to form 1 UTP and 1 Pi (Fig. 3D).

When starch utilization was prevented, the import levels of K^+ and Cl^- remained the same, but in contrast to the WT, some of the K^+ and Cl^- accumulated in the cytosol as a substitute for the glucose produced from starch in WT (Fig. 3, A and B). K^+ and Cl^- import to the vacuole decreased by 55% compared to the WT. Instead, there was a 5-fold increase in the degradation of sucrose that had been stored in the vacuole overnight into hexoses which then contributed to osmoticum. As in the WT, energy came from photosynthesis and was used for import of K^+ and Cl^- ions and for carbon fixation, but with more ATP utilized to fix carbon as less energy was used to transport K^+ and Cl^- across the tonoplast compared to the WT. In the starch knockout mutant, PP_i from the alternative Calvin–Benson–Bassham cycle flux mode was used by the tonoplast H^+-pyrophosphatase to energize the tonoplast for ion transport into the vacuole.

Starch breakdown provides both energy and osmoticum in nonphotosynthetic guard cells in white light stomatal opening

In the previous white light opening scenario, the assumed photosynthetic capacity of the guard cell was sufficient for the guard cell to function independently of carbon from the mesophyll. However, the capacity of the guard cell to perform photosynthesis

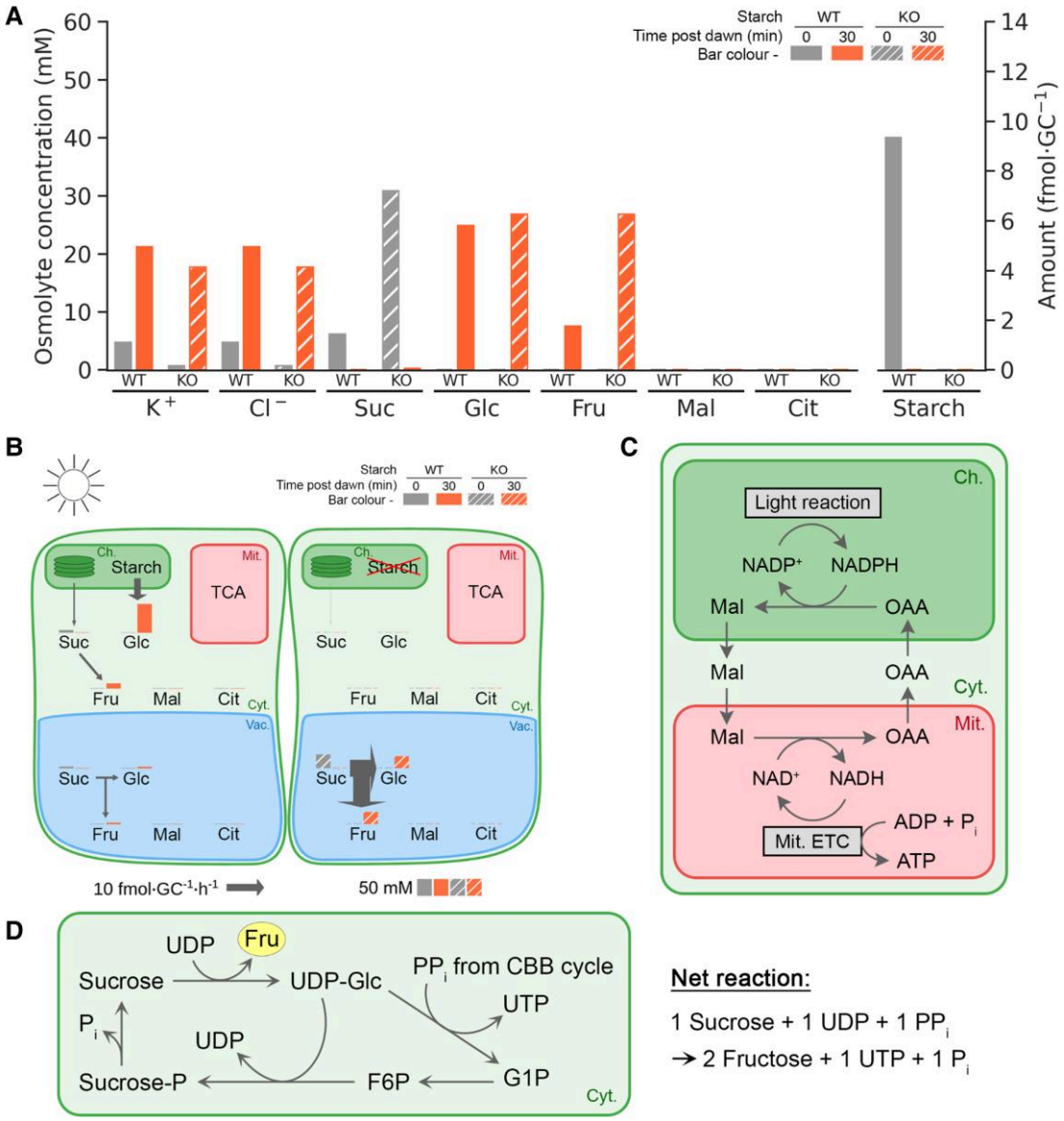

Figure 3. Osmolyte concentrations and metabolic fluxes in the guard cell during opening in white light. **A)** Overall concentration of osmolytes and amount of starch per guard cell in WT and starch knockout mutant. **B)** Bars show compartment-specific concentrations of organic osmolytes and arrows show metabolic fluxes, with the width of the arrows scaled linearly to flux. **C)** Flux mode for the shuttling of reducing power to the mitochondrion and the production of ATP by the mitochondrial electron transport chain. **D)** Flux mode for the utilization of PPi produced during carbon fixation in the WT simulation. Circled metabolites represent osmotica for stomatal opening. CBB cycle, Calvin–Benson–Bassham cycle; Ch., chloroplast; Cit, citrate; Cyt., cytosol; ETC, electron transport chain; Fru, fructose; GC, guard cell; Glc, glucose; KO, knockout; Mal, malate; Mit., mitochondrion; Suc, sucrose; TCA, tricarboxylic acid cycle; Vac., vacuole; WT, wild type.

is a matter of debate (Lim et al. 2022), so next we simulated a white light opening scenario where guard cells had no capacity for photosynthesis but, distinct from blue light opening, the mesophyll was able to perform photosynthesis as normal.

In the WT, import of K^+/Cl^- from the apoplast was still the most efficient way to increase osmolarity (Fig. 4A; for full results, see Supplementary Data Set 2). Import levels were in line with previous solutions, and all K^+/Cl^- was imported into the vacuole. The next largest contribution came from glucose in the cytosol and in the vacuole. About half of the cytosolic glucose was derived from starch breakdown and the rest from the breakdown of sucrose. This sucrose was stored overnight in the cytosol and 64% was degraded in the cytosol into glucose and fructose with the rest being imported to the vacuole for degradation. It was recently suggested that guard cells run a sucrose futile cycle during the later hours of the day to avoid excess starch synthesis while maintaining a pool of cytosolic sugars available to fuel glycolysis and mitochondrial metabolism if needed (Robaina-Estévez et al. 2017; Piro et al. 2023). Our model prevents futile cycles due to the pFBA formulation which minimizes the sum of metabolic fluxes. However, in alternative optimal solutions with relaxed constraints on metabolic flux sums, a futile cycle could explain the maintenance of high sucrose levels.

In the previous blue light and white light opening scenarios, the fate of glucose produced by starch breakdown was exclusively to accumulate as osmoticum, with no onward metabolism by glycolysis. Here, in contrast, 12% of the maltose released by starch breakdown was metabolized by an alpha-glucanotransferase into a 1:1 ratio of glucose and heteroglycans and the latter entered glycolysis via their catabolism into glucose 1-P. Thus, a full glycolytic

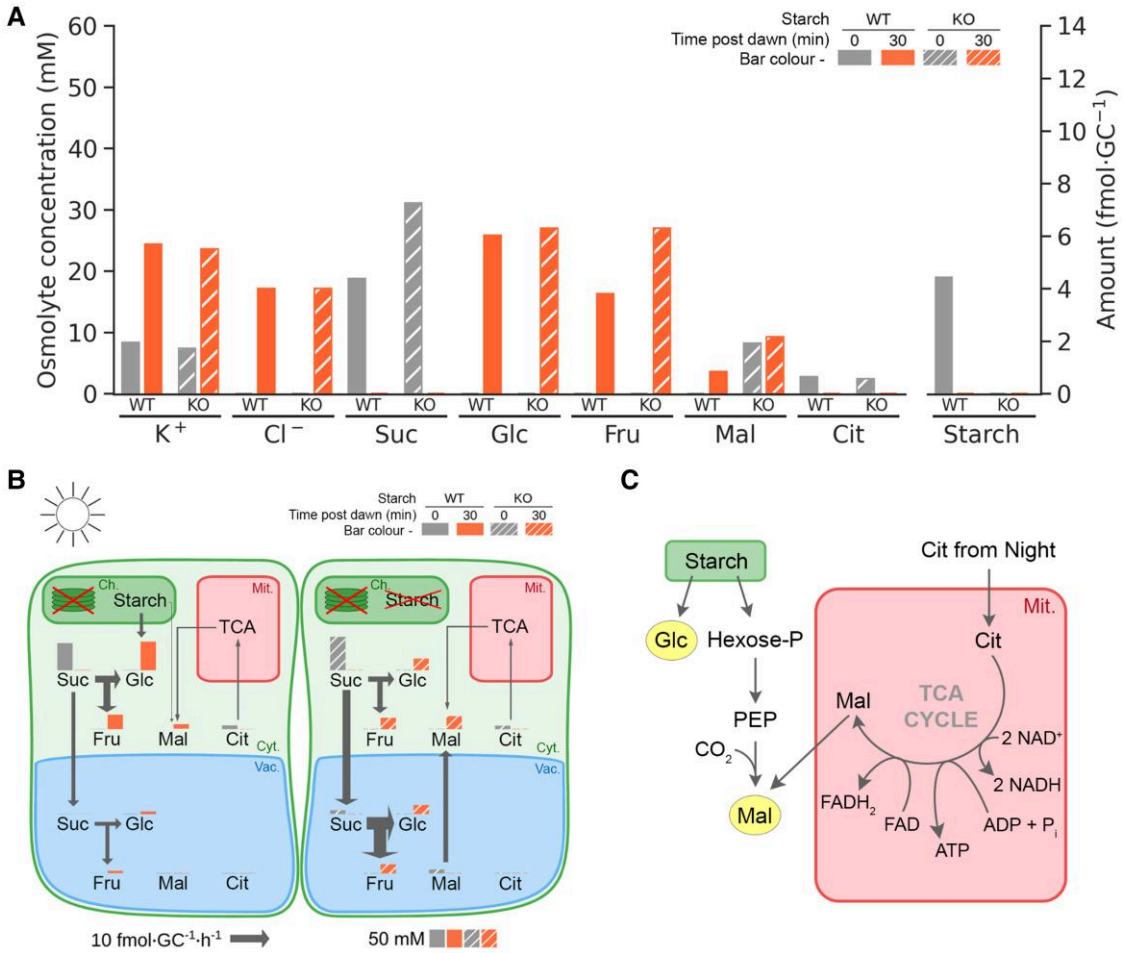

Figure 4. Osmolyte concentrations and metabolic fluxes in nonphotosynthetic guard cells during opening in white light. **A)** Overall concentration of osmolytes and amount of starch per guard cell in WT and starch knockout mutant. **B)** Bars show compartment-specific concentrations of organic osmolytes, and arrows show metabolic fluxes, with the width of the arrows scaled linearly to flux. **C)** The flux mode for the production of glucose and malate as osmotica in nonphotosynthetic guard cells during opening. Circled metabolites represent osmotica for stomatal opening. Ch., chloroplast; Cit, citrate; Cyt., cytosol; Fru, fructose; GC, guard cell; Glc, glucose; KO, knockout; Mal, malate; Mit., mitochondrion; Suc, sucrose; TCA, tricarboxylic acid cycle; Vac., vacuole; WT, wild type.

pathway was active as far as phospho*enol*pyruvate (PEP) (Fig. 4C). This metabolic shift to using glycolysis for energy and osmolyte production occurs when guard cell photosynthesis falls below 0.32% of that of the mesophyll cell per cell volume (Supplementary Fig. S4). PEP was then converted to malate via PEP carboxylase, which carried out anaplerotic carbon fixation as well as producing osmoticum in the cytosol. As in blue light, a partial TCA cycle in the guard cell converted citrate that had been stored in the cytosol overnight to malate. Malate was then exported to the cytosol for osmoticum (Fig. 4C) and the reducing power produced by the TCA cycle was used for ATP synthesis by oxidative phosphorylation.

The fluxes in this scenario are likely driven by the tradeoff between efficiently producing enough energy for import of K^+ and Cl^- while still retaining osmoticum. The partial breakdown of starch to malate produced energy from glycolysis while still producing osmoticum. Similarly, the conversion of citrate to malate using an incomplete TCA cycle created reducing power while not consuming osmoticum.

In the starch knockout mutant, K^+/Cl^- was imported into the guard cell at the same level as in the WT simulation, and while all the Cl^- was transferred into the vacuole, 71% of the K^+ remained in the cytosol to compensate for the loss of starch-derived osmotic sugar (Fig. 4, A and B). A larger proportion of the vacuolar osmolarity was provided through partial import of sucrose that had been stored overnight in the cytosol and its subsequent degradation into hexoses. The level of this vacuolar degradation was around 3-fold higher than in the WT. Malate was transferred from the vacuole to the cytosol, balancing the flow of negative charge of Cl^- into the vacuole. Sucrose was also catabolized in the cytosol at 77% of the level in WT. As starch could not be utilized, energy was solely provided by the conversion of citrate to malate via an incomplete TCA cycle. This led to a lower rate of energy production which was offset by a 26% decrease in consumption from the tonoplastic H^+-ATPase pump. This decrease was achieved partly through replacing the import of K^+ ions into the vacuole with import of sucrose and its subsequent degradation into glucose and fructose.

These simulations showed that starch could be converted to glucose and malate during opening to provide a mixture of osmoticum and energy. The latter required glycolysis, which was in contrast to the white light opening scenario where energy needs were met by guard cell photosynthesis in the absence of glycolysis. Thus, the necessity for glycolysis depended upon the extent to which guard cell photosynthetic capacity could meet the energy demand for stomatal opening. Moreover, without guard cell photosynthesis, the role of malate changed from being a conduit

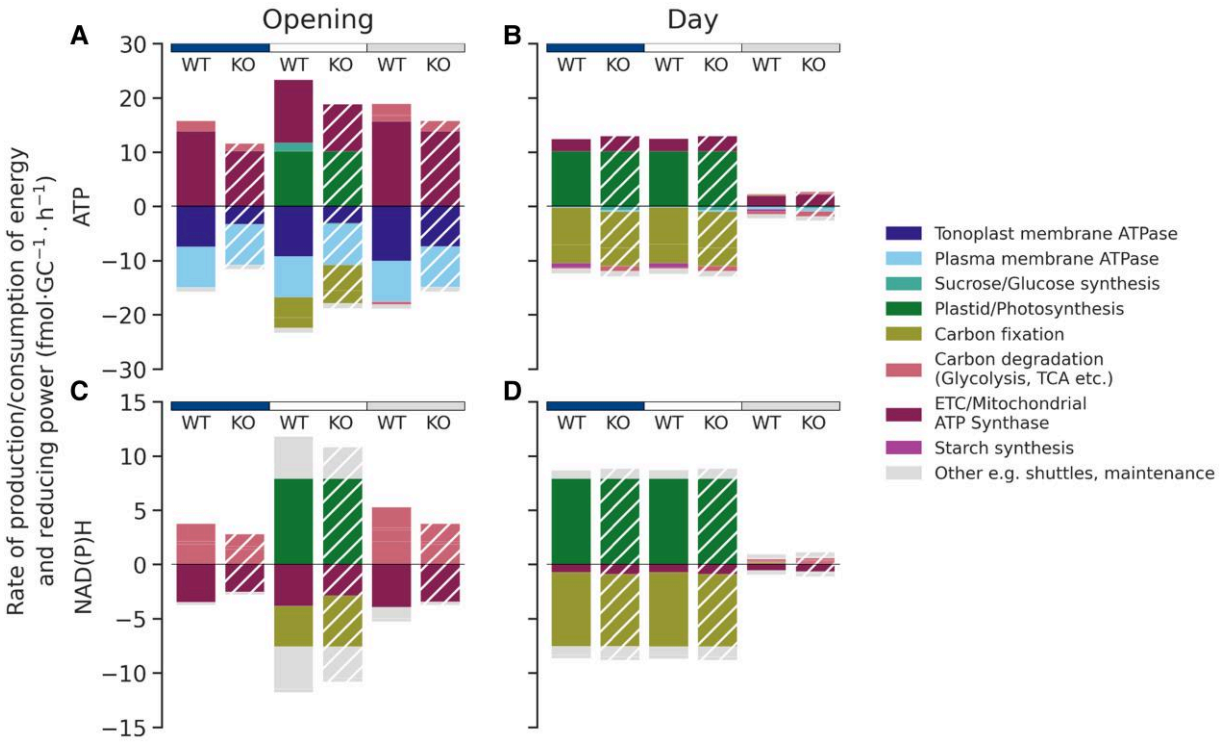

Figure 5. Energy and reducing power budgets for the guard cell during opening and day phases for different scenarios. The color above the bars indicates the simulated light condition, with blue, white, and gray indicating that the guard cell was in blue light, in white light, and nonphotosynthetic, respectively. Labels below the light condition indicators represent wild-type (WT) or starch degradation knockout mutants (KO). The amount of ATP **A, B)** and NAD(P)H **C, D)** produced and consumed for the 6 scenarios analyzed during the opening **A, C)** and day **B, D)** phases. Fluxes which produce ATP or NAD(P)H are above 0 and fluxes which consume ATP or NAD(P)H are below 0. Fluxes are grouped according to metabolic categories. For the list of the reactions and their respective categories, see Supplementary Data Set 3.

for transfer of reducing equivalents between chloroplast and mitochondrion to being used as an osmolyte.

Preventing guard cell starch utilization leads to lower ATP turnover during opening but a less carbon-efficient leaf overall

The simulations show that guard cell metabolism can be flexible and operate in different modes depending on the environmental and biological constraints. To obtain a detailed overview of the cellular economy, we investigated the energy and carbon budgets of the opening and day phases of the guard cell in the 6 scenarios we have described (Figs. 5 and 6 and Supplementary Data Set 3, for full results, see Supplementary Data Set 2). This analysis highlights the importance of including both day and night temporal phases and interactions with the mesophyll cell in the model, as the turnover of ATP and NAD(P)H in the opening phase did not necessarily associate with the overall efficiency, measured as phloem output over the diel cycle.

During opening, the highest guard cell ATP turnover occurred in the white light scenarios due to the large production of ATP by photosynthesis and its consumption for carbon fixation (Fig. 5A). In the absence of photosynthesis, ATP production was largely dependent on the mitochondrial ATP synthase with only minor contributions from substrate level phosphorylation and glycolysis. Proton pumping by the plasma membrane H^+-ATPase took its maximum constrained value in all 3 scenarios and it was the main consumer of ATP during blue light opening. The involvement of the tonoplast varied between the 3 scenarios, and this contribution decreased in the starch knockout scenarios in which the accumulation of sucrose in the vacuole in place of starch led to more vacuolar sugars as osmoticum and less transport of K^+ and Cl^- across the tonoplast.

During the day, all scenarios with photosynthetic capacity produced the same level of ATP mainly through photosynthesis and this was mostly consumed by carbon fixation in the Calvin–Benson–Bassham cycle (Fig. 5B). In the scenario with no photosynthetic capacity, the vast majority of ATP was produced by the mitochondrial ATP synthase, and then consumed by the plasma membrane H^+-ATPase to import sucrose as well as for maintenance.

During opening, all the NAD(P)H was generated from oxidative metabolism except in the white light scenario where most of the NAD(P)H was derived from photosynthesis (Fig. 5C). Besides carbon fixation and maintenance, the reducing power was almost all consumed by the mitochondrial ATP synthase.

During the day, in scenarios with photosynthesis, NAD(P)H was generated through photosynthesis and used for carbon fixation (Fig. 5D). NAD(P)H turnover in the scenario without photosynthetic capacity was about 12% of the other scenarios, with reducing power generated via glycolysis and the TCA cycle mostly used for ATP production in the mitochondrial electron transport chain and for maintenance.

The metabolic efficiency of the guard cell can be judged by considering the net export of carbon from the guard cell to the mesophyll cell. There was no transport of carbon between the 2 cell types during the opening phase under any scenario, so in the following, we refer only to the day phase (Fig. 6). The guard cell was a net exporter of carbon in the scenarios where it had photosynthetic capacity, and despite large differences in ATP and NAD(P)H production and consumption during opening, the export

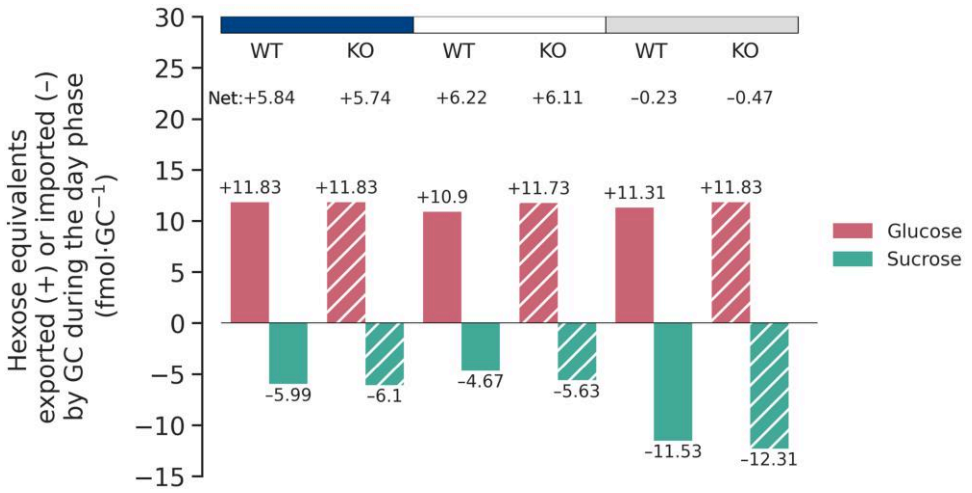

Figure 6. Carbon import and export of the guard cell during the day phase for different scenarios. The color above the bars indicates the simulated light condition, with blue, white, and gray indicating that the guard cell was in blue light, in white light, and nonphotosynthetic, respectively. Labels below the light condition indicators represent wild-type (WT) or starch degradation knockout mutants (KO). Transport of hexose equivalents per guard cell during the day phase for the 6 scenarios analyzed. Total export over the phase is represented by a stacked bar with a positive number above it and total import with a stacked bar with negative number below it. The net value of export (+) or import (–) is given above the pair of bars.

levels were similar for these scenarios. In the blue light and white light opening scenarios, the guard cell imported sucrose and exported glucose, with roughly twice the amount of carbon exported than imported, resulting in a net export of carbon. In the white light scenario, net carbon export was 6.5% higher compared to the blue light scenario as the guard cell received extra energy from photosynthesis. This net carbon export decreased by 1.8% when starch could not be utilized in the starch-breakdown mutant in white light.

The guard cell was a net importer of sugars in the scenarios without guard cell photosynthesis. In both the WT and the starch knockout, the export of glucose was similar to that in scenarios with guard cell photosynthesis, but the import of sucrose was higher, resulting in a small net import of carbon (Fig. 6). In the WT, 11.53 fmol·GC^{-1} of hexose equivalents of sucrose was imported compared to 11.31 fmol·GC^{-1} glucose exported, a difference of 0.23 fmol·GC^{-1}. The net sugar import was about doubled in the starch knockout, presumably due to the lack of starch breakdown for energy production.

In summary, this analysis demonstrates that in many instances, a higher energy turnover in the opening phase results in a more efficient guard cell overall. It also shows that the cost of opening and closing of the guard cell is comparable to the estimated guard cell photosynthetic capacity.

Conclusions are insensitive to variation in parameters or enzyme/transporter costs

There is considerable variation in guard cell physiology across different species, and in addition, there was uncertainty in the values to be used for parameters in the selected scenarios. To confirm that our conclusions were robust to variations in these parameters, we performed a parameter sensitivity analysis on the 19 parameters in the model (Table 1, excluding PPFD where all other parameters were varied relative to PPFD). As testing of all combinations with only 2 levels of each parameter would have led to $2^{19} = 524{,}288$ simulations, we performed a parameter sampling. This allows a systematic sampling from a high dimensional parameter space to generate a computationally manageable number of parameter sets representative of the whole parameter space. In our case, we chose reasonable bounds for the 19 parameters (Supplementary Table S2) and used Latin hypercube sampling to generate 1,000 parameter combinations for further analysis. Of these 1,000 parameter sets, 968 resulted in sensible constraints with 32 combinations removed due to the open aperture being smaller than the closed aperture. We simulated the model using each of the 968 parameter sets under both blue and white light opening and obtained a total of 1,934 solutions and 2 infeasible simulation. Figure 7 displays the results of this parameter sampling. The constraints used are available in Supplementary Data Set 4, and the results for blue and white light opening in Supplementary Data Sets S5 and S6, respectively.

We first investigated how much each parameter affected phloem output of the leaf. To relate the parameters of the model with phloem output of the leaf, we used lasso regression to fit a linear model (see Materials and methods). Using only the proportion of photons absorbed by the leaf (P_{abs}) and whether opening was in blue or white light, the linear model predicted phloem output with an $R^2 > 0.999$ (Fig. 7A), suggesting that the phloem output is mostly dependent on incident light. As this output is very sensitive to parameters that are not directly related to the guard cell, we repeated the lasso regression to fit a model relating net hexose export from the guard cell with a reduced set of parameters more specific to the guard cell including the volume and osmolarity of the guard cell when opened and closed, the photon influx into the guard cell, and the upper bound of the plasma membrane H^+-ATPase in the guard cell. To correct for blue versus white light opening, we multiplied the photon influx by the number of hours for which it occurred (11.5 for blue and 12 for white light opening) to give photon influx per day into the guard cell. The net hexose export was correlated with daily photon influx into the guard cell with an R^2 of 0.952, and combining this with the difference in osmolarity upon opening improved it further to 0.998 (Fig. 7B). Importantly, the guard cell acted as a source tissue in 1,757 out of 1,934 (91%) feasible solutions, suggesting that in most scenarios, guard cells are not a sink tissue.

Our model initially overestimated the flux of plasma membrane H^+-ATPase and so the flux was constrained to the value calculated from the OnGuard model. We investigated the impact of variation in the kinetics of the plasma membrane H^+-ATPase

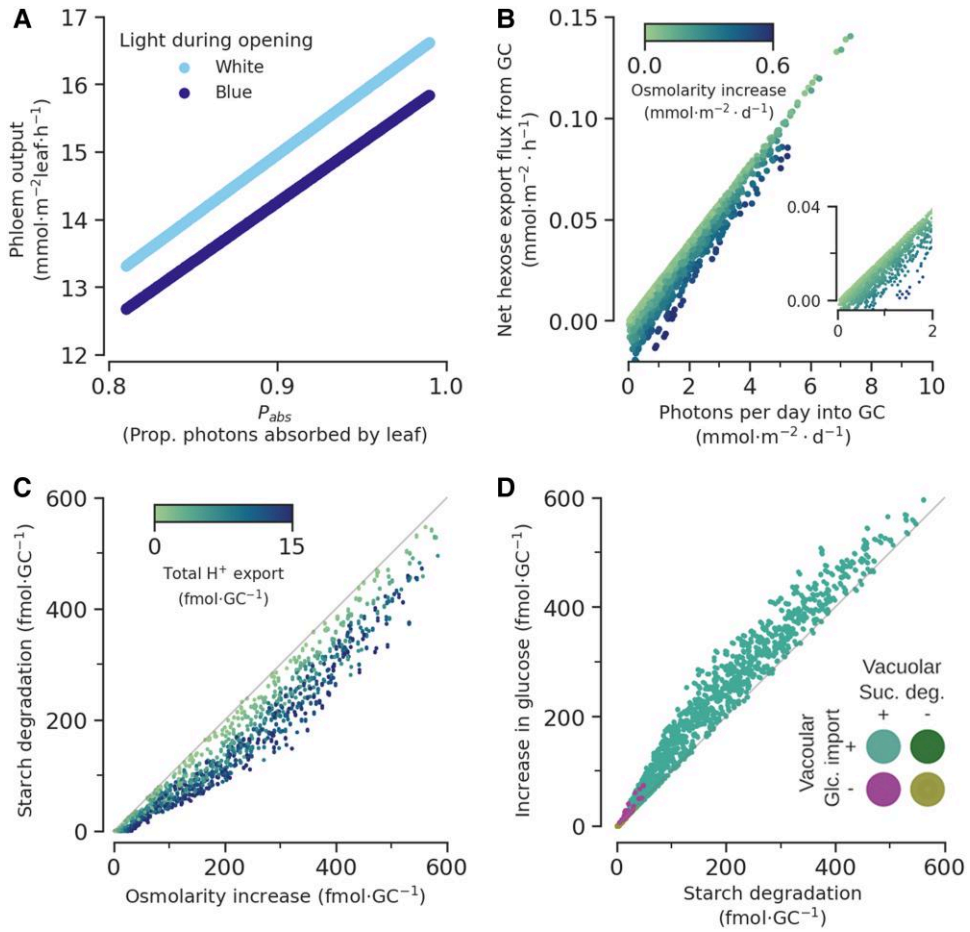

Figure 7. Effect of varying model parameters on guard cell starch and sugar metabolism. We selected 965 feasible of 1,000 combinations of the 19 model parameters that were variable, using Latin hypercube sampling with bounds as given in Supplementary Table S2. Each dot in the plots represents the solution for 1 combination of parameters and blue and white light, respectively. **A)** Phloem output versus P_{abs}, the proportion of photons that hit the leaf that are absorbed, colored by whether the opening is in blue or white light. **B)** Net hexose export versus total photons into the guard cell across the diel cycle. Color corresponds to the total osmolarity increase of the guard cell. **C)** Guard cell starch degradation versus the increase in osmolarity during opening, colored by the total level of H^+ export by plasma membrane H^+-ATPase. The gray line represents a 1:1 relationship between osmolarity increase and starch degradation. **D)** Increase in total guard-cellular glucose during opening versus the level of starch degradation per guard cell during opening. Colors indicate whether glucose was imported from the cytosol into the vacuole (Vacuolar Glc. import) and whether sucrose is degraded in the guard cell (Vacuolar Suc. deg.). The gray line represents a 1:1 relationship between starch degradation and increase in glucose.

and found that it had relatively small effects on the energetics of the guard cell, with the flux only correlated to hexose export with an R^2 of 0.109. Despite this, we wanted to test its influence on guard cell flux modes and particularly on the utilization of starch. In 98% of solutions, starch was degraded in the guard cell during opening, indicating that its utilization is a crucial component of optimal opening. Starch utilization was almost completely controlled by whether the upper bound set on the plasma membrane H^+-ATPase was limiting, i.e. whether the import of K^+ and Cl^- was sufficient for the change in stomatal aperture. The plasma membrane H^+-ATPase activity was limiting for 98.5% of the 1,892 solutions utilizing starch, while the plasma membrane H^+-ATPase activity was not limiting in all 42 solutions without starch utilization. These results suggest that the import of K^+ and Cl^- energized by plasma membrane H^+-ATPase was the preferred way of generating osmotic pressure and only when the import of K^+ and Cl^- was insufficient starch was broken down to produce osmoticum. The level of starch degradation can be determined largely by a combination of the total increase in osmolarity upon opening and the level of flux permitted through the plasma membrane H^+-ATPase, especially at lower osmolarity increases (Fig. 7C).

Subsequently, we investigated the 1,892 solutions where starch was degraded to explore its utilization pattern. We assumed that the degradation of starch via the amylolytic pathway, which generates only glucose molecules, was driven primarily by the need to produce osmoticum. On the other hand, when starch was degraded to form 1 glucose molecule and 1 glucose 1-phosphate molecule, we assumed that the driver was energy production, with half of the energy utilized for glycolysis and the remaining half retained as glucose for osmoticum. In white light, starch was used for production of osmoticum in all solutions, but for energy production in only 37% of solutions. Even in the solutions where starch was used for energy, only an average of 3.4% of the starch was degraded for energy with most of the starch used for producing osmoticum. For blue light, while the majority (96%) of solutions used starch for energy, on average only 7% of the starch was degraded for energy. This reinforced the conclusion that the main driver for starch utilization was the production of osmoticum.

As we and Flütsch et al. (2020) have both observed starch being utilized for glucose during the opening process, we conducted a comparison between starch degradation and the concurrent

increase in glucose concentration (Fig. 7D). We observed a strong positive relationship between starch degradation and the net increase in glucose concentration during stomatal opening. The solution can be separated into 4 different categories depending on the presence or absence of sucrose degradation in the vacuole and glucose import into the vacuole. For solutions with a low glucose increase, presumably corresponding to a low osmoticum requirement and/or high upper bound on the plasma membrane H^+-ATPase, starch degradation was sufficient to provide glucose as osmoticum in the cytosol without the need to import glucose into the vacuole (6.0% of solutions). As glucose accumulation increased, sucrose degradation in the vacuole was needed to produce hexoses for osmoticum in the vacuole without glucose import into the vacuole (2.5% of solutions). At higher glucose accumulation and starch degradation, glucose produced from starch was imported into the vacuole, with most of the solutions also involving sucrose degradation in the vacuole (90.9% of solutions) and only 12 solutions (0.6% of solutions) with glucose import without vacuolar sucrose degradation. These results suggest that starch degradation is important in producing glucose as osmoticum, with some of the resulting glucose being transported into the vacuole in most cases. Furthermore, this process can be accompanied by the degradation of sucrose stored overnight to produce hexoses as osmoticum in the vacuole.

In summary, based on this comprehensive robustness analysis, we can conclude that the results obtained for the selected scenarios (Figs. 2 to 4) provide a reliable representation of the potential flux modes, despite the uncertainties surrounding the precise parameter values used. We found that the guard cell is likely to act as a source tissue unless photosynthetic capacity is very small relative to the mesophyll cell, and that the kinetics of the plasma membrane H^+-ATPase and the resulting limited import of K^+ and Cl^- are likely to be a key point of control for starch utilization. The key driver for starch utilization is likely the production of glucose for osmoticum, rather than provision of energy.

Discussion

The stoichiometric integrated guard cell metabolic model presented here predicts metabolic and osmolyte fluxes taking into consideration the interaction with the mesophyll and the day and night cycle of leaf metabolism under the assumption that stomatal opening is realized in a way that maximizes the overall performance of the leaf. The model partially builds on, and complements, the OnGuard model (Hills et al. 2012) which enables dynamic simulations of ion transport processes at the plasma membrane and tonoplast in the guard cell. Furthermore, the model overcomes some of the weaknesses of previous stoichiometric models of guard cell metabolism such as limitation to a single metabolic state (Robaina-Estévez et al. 2017), the lack of consideration of the guard cell mesophyll interaction, and rigid constraints that enforce the model predictions to match experimental observations (Robaina-Estévez et al. 2017; Tan and Cheung 2020).

Guard cell starch breakdown during stomatal opening is for osmoticum and not energy production under different light conditions

Analysis of the levels of sugars and malate in guard cells isolated from wild type and α-amylase3 (AMY3) and β-amylase1 (BAM1) knockout mutants suggests that the role of blue light starch turnover is to provide sugars and not malate (Flutsch et al. 2020). Stoichiometric modeling not only confirms this observation, but explains why: It is the most efficient way to provide organic osmoticum in the cytosol in the absence of photosynthesis. Meanwhile, the metabolism of a small amount of citrate stored overnight can entirely meet the energy needs of the guard cell via mitochondrial metabolism. Moreover, even in white light opening (i.e. in the presence of photosynthesis), if starch is present, then it is mobilized to generate sugars that contribute to the osmotic requirement for guard cell expansion. Interestingly, the model predicts that starch-derived glucose accumulates in the cytosol and not the vacuole, where import of K^+ and Cl^- remains the most energy efficient mechanism for increasing turgor. In the absence of starch breakdown, the model reveals that the next most efficient route to guard cell expansion is to retain a greater proportion of imported KCl in the cytosol and to generate vacuolar turgor by hydrolysis of sucrose stored overnight to generate 2 hexoses.

Use of sugars as cytosolic osmoticum for stomatal opening

Although the prediction of the model that glucose derived from starch turnover in blue light accumulates as a cytosolic osmoticum is consistent with results from Arabidopsis starch turnover mutants (Flutsch et al. 2020), it is also possible for the other cytosolic product of starch breakdown, maltose, to contribute to cytosolic osmoticum. However, as demonstrated by the model, it is more efficient from an osmotic standpoint to cleave the maltose into 2 glucose molecules, which raises the question as to why maltose has been observed to accumulate in broad bean (*V. faba*) epidermal peels exposed to blue light (Talbott and Zeiger 1993).

One possible explanation could be regulatory: It has been demonstrated that high levels of sugars stimulated stomatal closure in a response mediated by the hexokinase sugar sensor and a number of other signaling systems (Kelly et al. 2013; Li et al. 2016; Hei et al. 2017; Kottapalli et al. 2018). Therefore, the use of sugars such as glucose as an osmoticum to drive stomatal opening could be counterproductive if the sugar instead signals the induction of stomatal closure. The accumulation of maltose as an osmolyte would potentially avoid hexokinase-mediated sugar signaling as long as the maltose was not further metabolized to glucose. As our model does not capture these regulatory considerations, it chooses to use the more-osmotically efficient solution of glucose accumulation. Nevertheless, if hexose accumulation is prevented in the model, then it does indeed elect to accumulate starch-derived maltose as a cytosolic osmoticum, with a minor penalty in terms of the overall efficiency of the system (1%).

Note that while maltose is the primary product of transitory starch breakdown in leaves, maltotriose is also produced as a product of glucan chains with odd numbers of glucose residues and is acted on by chloroplast disproportionating enzyme to generate maltopentaose and glucose (Critchley et al. 2001). Some of this glucose is likely to be exported to the cytosol and thus it is conceivable that even with no onward metabolism of maltose, some cytosolic glucose will be generated by starch breakdown. It is unclear whether this glucose could accumulate to levels that are insufficient to trigger hexokinase-mediated signaling or whether it would have to be metabolized by glycolysis.

The use of glycolysis in guard cells

However one views it, in order for either maltose or glucose to accumulate to contribute to cytosolic osmoticum, there would have to be limited onward metabolism of the sugars otherwise they would not accumulate. The limited role for guard cell glycolysis during blue- and white-light opening in the model is consistent

with this, but is nevertheless one of the more striking predictions of our model. The model demonstrates that, in principle, guard cell glycolysis is not necessary to support the energy requirements of stomatal opening. In blue light-induced opening, the guard cell was energized in the model by a pattern of carboxylic acid metabolism that involved a citrate–malate cycle over the diel cycle. Citrate is metabolized to form malate by a partial TCA cycle during stomatal opening while malate accumulates throughout the day and is converted back into citrate at night. The citrate–malate cycle allows the guard cell to "shuttle" energy over the diel cycle without affecting the overall osmoticum level, which could be particularly important in guard cells. Although further experimental work would be required to test this prediction, we note that malate has been observed to accumulate in epidermal peels exposed to blue light (Talbott and Zeiger 1993).

In white light-induced stomatal opening, when guard cell photosynthesis was allowed to be active in the model, the chloroplast and mitochondria coordinately provided the energy required for opening. As much of that energy is required in the cytosol and the chloroplast lacks an active ATP export system (Shameer et al. 2019; Lim et al. 2022), cytosolic ATP was predicted to be supplied via mitochondrial oxidative phosphorylation which was powered by malate exported from the chloroplast. Again, in this scenario, glycolysis was not required. This is in apparent contradiction to experimental evidence that suggests that guard cell glycolysis is stimulated by illumination (Hedrich et al. 1985). The experimental evidence is based on the observed increase of the regulatory metabolite fructose 2,6-bisphosphate which would lead to stimulation of glycolysis by activation of the enzyme PFP and by inhibition of the gluconeogenic enzyme fructose-1,6-bisphosphatase. A decline in hexose phosphate levels was observed upon illumination of isolated guard cell protoplasts from *V. faba* which could also be consistent with an acceleration of glycolysis. However, we note that no flux measurements were made and the results are open to interpretation.

Moreover, it is also apparent from our model that the extent to which glycolysis contributes to energy metabolism during stomatal opening is crucially dependent on the capacity for guard cell photosynthesis, something that remains much debated. We show that if guard cell photosynthesis drops below a certain threshold (in our model, this is expressed in terms of the relative total volume of guard cell chloroplasts versus mesophyll chloroplasts and the crucial threshold is 0.32%—see Supplementary Fig. S4), then guard cell glycolysis becomes important. Also, under this threshold, PEP carboxylase also becomes active in the model. While these results appear more consistent with the interpretations of metabolic activity in guard cells based on ^{13}C-labeling experiments of guard-cell-enriched epidermal fragments of tobacco (*Nicotiana tabacum*) leaves (Daloso et al. 2015), the sensitivity of guard cell metabolism to the extent of guard cell photosynthesis and the nonphysiological state of the guard cells in the labeling experiments raises the possibility of alternative flux modes in vivo in which glycolysis and PEP carboxylase are less important. The experimental literature presents contradictory evidence about the role of photosynthesis in guard cells, with some studies demonstrating that the absence of guard cell chloroplasts attenuates stomatal responses (Wang et al. 2014) and others suggesting that guard cell chloroplasts have a limited role in stomatal energy metabolism (Lim et al. 2022).

If guard cell photosynthesis is sufficiently active that glycolysis becomes less important to energize stomatal opening, then how do we reconcile the fact that transcriptomic data and ^{13}C-labeling studies both suggest that the enzymes of glycolysis are present and can be active to generate an appreciable flux (Medeiros et al. 2018)? The answer is that despite not being substantially important in the model during stomatal opening, the model does predict substantial glycolytic flux at other times of the day and, in all scenarios tested, glycolysis was active at night where it played a major role in energy provision by substrate level phosphorylation (Supplementary Data Set 2).

Guard cells are likely to act as a source tissue

The ongoing discussion about the photosynthetic activity of guard cells and the contribution it makes to stomatal opening (Flütsch et al. 2022, Lemonnier and Lawson 2024) and our demonstration of the sensitivity of metabolism to the extent of guard cell photosynthesis means that it remains unclear what are the dominant metabolic flux modes that support guard cell energy metabolism. Guard cells usually contain chloroplasts and all the enzymes of the Calvin–Benson–Bassham cycle (Lawson et al. 2014; Lawson and Blatt 2014). However, the chloroplasts are typically smaller and less numerous than in mesophyll cells and the levels of Rubisco are relatively low (Outlaw 1989; Vavasseur and Raghavendra 2005). At the same time, guard cells contain large numbers of mitochondria (Allaway and Setterfield 1972) and experiments on guard cell protoplasts suggest that mitochondrial oxidative phosphorylation is the main source of energy in guard cells (Lim et al. 2022). These observations raise questions about the quantitative importance of guard cell photosynthesis (Santelia and Lawson 2016). Recent work showed that although the role of photosynthesis in guard cells might be small, chlorophyll at the thylakoid membrane seems to be critical for guard cell turgor (Lim et al. 2022). They also found that guard cell photosynthesis is required for proper starch accumulation in guard cell chloroplasts which is in line with previous reports (Azoulay-Shemer et al. 2015).

In this study, the model was parameterized using anatomical and photosynthetic data from the literature for Arabidopsis and guard cells with photosynthetic activity were net exporters of carbohydrate during the day phase (Fig. 6). The effect of varying the photosynthetic capacity of the guard cell was tested using a constraint sampling strategy and this showed that even a very low level of photosynthesis compared to the mesophyll would be sufficient for guard cell functioning over the whole diel cycle (Fig. 7). On this basis, we conclude that it is most likely that the guard cell acts as a source tissue, with photosynthetic carbon fixation making a major contribution to its energy budget and carbon metabolism during the day. Evidence for photosynthetic carbon fixation in guard cell chloroplasts has been obtained in ^{13}C-bicarbonate labeling experiments (Daloso et al. 2015).

Recently, it has been suggested from a meta-analysis of the ^{13}C-labeling patterns observed in experiments in which leaves and epidermal strips were incubated with $^{13}CO_2$, ^{13}C-bicarbonate, and ^{13}C-sucrose that guard cell metabolism has the characteristics of a sink tissue (Daubermann et al. 2024). However, in contrast to the modeling analysis, the labeling experiments have not yet yielded quantitative measures of the fluxes through the guard cell network, and this limits the extent to which conclusions can be drawn about the contribution of the detected pathways to the overall energetics and carbon balance of the guard cell. As a further complication, the supply of CO_2 from ^{13}C-bicarbonate solution is unlikely to match that which the guard cell would experience via the stomata in a leaf and that could compromise the overall contribution of photosynthesis to metabolism in the experiments.

Limitations of the model

As in any stoichiometric model that predicts metabolic fluxes based on an optimality principle, the model includes only minimal manually curated information about kinetic constraints and does not explicitly account for enzyme kinetics. Hence, it may be that regulatory or enzyme-capacity limitations could lead to different metabolic flux modes to the ones we predict. The model in its current formulation is also not capable of predicting impaired stomatal dynamics (either with respect to aperture or the time it takes to open) as these data are inputs for the model. However, as we demonstrate, parameter scans can be used to explore the effect of varying the relationship between aperture and osmolarity. While the modeling framework itself could readily be adjusted to accommodate a more fine-grained temporal resolution, the analysis of each in silico experiment needs a detailed consideration of flux distributions in 2 cell types and multiple time intervals. Thus, a more detailed analysis of metabolism and the fate of osmolytes during the rest of the day would go beyond the scope of this study. On a related note, the model did not choose fatty acids for the production of respiratory substrates as shown for guard cells of Arabidopsis plants grown under short day conditions and/or heat stress (McLachlan et al. 2016). Further studies could investigate under which specific conditions the utilization of lipids might be favorable.

Conclusions

Our modeling work revealed a range of different metabolic behaviors in the guard cell, some of which are quite different to the dominant (and therefore expected) flux modes observed in other tissues. The work resolved the role of starch breakdown during blue light opening: It is the most efficient way of contributing to cytosolic osmoticum by accumulation of glucose. Moreover, the modeling suggested that mechanistically, this is achieved by downregulation of guard cell glycolysis. The interplay between citrate and malate could play a role in supporting the energetic needs of guard cells while maintaining osmotic pressure. In white light opening, a coordinated action of chloroplast and mitochondrial metabolism, connected by a malate shuttle, provided energy for guard cell ion and metabolite transport. These varying and in many cases unusual flux modes demonstrate the flexibility of guard cell metabolism to efficiently realize stomatal opening in various environments. With our analyses, we have been able to corroborate some of the recent findings in Arabidopsis guard cell research, demonstrated the validity of our conclusions with respect to variation in parameters or enzyme/transporter costs, helped to resolve conflicting experimental observations by demonstrating the flexibility of guard cell metabolism, and put forward metabolic flux modes for further experimental testing.

Materials and methods

The code required to reproduce the results presented here, including most of the figures, is available as Jupyter notebooks at https://github.com/toepfer-lab/mmon-gcm, with documentation at https://toepfer-lab.github.io/mmon-gcm/. Please refer to this for the most complete and accurate description.

Constructing an integrated stoichiometric model of guard cell and mesophyll metabolism with 4 temporal phases

The starting point for the model of guard cell metabolism was our previously published stoichiometric model of plant central metabolism, PlantCoreMetabolism_v1_2 (Shameer et al. 2018). This core model was duplicated to represent guard cell and mesophyll cell metabolism with the respective suffixes _gc and _me added to reaction identifiers. In the guard cell, reactions representing plasma membrane and tonoplast transporters and channels were added based on literature (Hills et al. 2012; Feng and Frommer 2015; Santelia and Lawson 2016) (Supplementary Fig. S2). For every metabolite or ion that contained transporters to the extracellular compartment, a "transfer reaction" was included in the mode to allow exchange between the extracellular compartment of the cell and the apoplast compartment (Supplementary Figure S1).

To represent stomatal aperture dynamics over the course of the diel cycle, the 2-cell model was quadrupled to represent 4 distinct time phases with additional suffixes of _1, _2, _3, and _4 added to reaction identifiers. The temporal phases were connected by "linker reactions" that allowed the simulation of the accumulation and degradation of specified metabolites by passing them from one time phase to the next. Because the model is required to balance fluxes across the complete day–night cycle, metabolites that accumulate in 1 or more phases must be consumed in subsequent phases. Linker reactions are defined in a .csv file that is parsed by the model creation scripts. Linker reactions for species with a mixed protonation state, such as malate and citrate, have the corresponding linker reactions for each protonation state added. Throughout the text, the use of malate and citrate refers to the sum of the 2 protonation states. The linker reactions included in the model are listed in Supplementary Table S1.

Scaling of fluxes to account for temporal differences

The inclusion of temporal phases of unequal duration is an extension of our previously described "diel" frameworks (Cheung et al. 2014; Töpfer et al. 2020) and necessitates appropriate scaling of linker fluxes. For example, if glucose for osmoticum is produced at a rate of 5 fmol·h^{-1}, 10 fmol will be produced if a phase is 2 h long, but only 2.5 fmol if the phase is 0.5 h long, and this also holds for rate of consumption in the next phase. Linker reactions were therefore constructed according to the following equation:

$$\text{Linker i:} 1/\text{Phaselength}_i \cdot \text{Species}_i -> 1/\text{Phaselength}_{i+1} \cdot \text{Species}_{i+1}.$$

For example, for Linker 2 (phase 2 is 0.5 h, phase 3 is 11.5 h): 2·Species -> 0.087·Species.

Charged pseudo-osmolytes were also added to linker reactions of charged species to ensure no net charge is accumulated across phases. Finally, total phloem output was calculated by multiplying the output flux of each temporal phase by the length of the phase and summing up the 4 phases.

Scaling of fluxes to account for cell size

Another important scaling consideration was the unequal total proportion of the 2 cell types in the leaf. This was taken into account by scaling the influx of photons into the 2 separate cell types relative to their volumes. We first define that all photons that are absorbed by the leaf contribute to either guard cell or mesophyll photosynthesis:

$$P = P_{abs} \cdot \text{PPFD}$$
$$P = P_{GC} + P_{MC}$$

where P is the total number of photons absorbed per m^2 of leaf; P_{abs} is the proportion of photons that hit the leaf that are absorbed, and PPFD is the number of photons that hit each m^2 of leaf. P_{GC} is the total photon uptake by the guard cell per m^2 of leaf; P_{MC} is the total photon uptake by the mesophyll per m^2 of leaf.

We then define guard cell photon influx to be the product of total influx (P), the proportion of the volume of the leaf that is guard cells ($Prop_{gc}$), and the efficiency (e) of guard cell photosynthesis compared to mesophyll:

$$P_{GC} = e \cdot Prop_{gc} \cdot P$$

where efficiency is the product of the quantum efficiency (F_qF_m), the number of chloroplasts in the guard cell relative to the mesophyll (R_{ch}), and the volume of chloroplasts in the guard cell relative to the mesophyll (R_{chvol}):

$$e = F_qF_m \cdot R_{ch} \cdot R_{chvol}.$$

The volume of the leaf (V_L), the total volume of guard cells (V_{gc}), the total volume of the mesophyll cells (V_{me}), and the proportion of the volume of the leaf that is guard cells ($Prop_{gc}$) are defined as:

$$V_L = T_L \cdot A_L$$
$$V_{gc} = V_{gcind} \cdot N_{gcs}$$
$$V_{me} = V_L \cdot (1 - Prop_{epidermis}) \cdot (1 - Prop_{air})$$
$$Prop_{gc} = V_{gc}/(V_{me} + V_{gc})$$

where T_L is the thickness of the leaf; A_L is the area of the leaf (which was set as 1 m^2 to study the metabolic fluxes per 1 m^2 leaf area); V_{gcind} is the volume of an individual guard cell; N_{gcs} is the number of guard cells; $Prop_{epidermis}$ is the proportion of the leaf that is epidermis; and $Prop_{air}$ is the proportion of the leaf that is air.

Assuming that the volume of the guard cell is negligible compared to the mesophyll cell:

$$Prop_{gc} = V_{gc}/V_{me}.$$

Thus, photon influx into the guard cell and mesophyll during the day can be constrained by specifying the relevant parameters outlined in Table 1. Photon input for the night phases was set to 0.

Phloem output reaction

We use the phloem output reaction defined earlier (Cheung et al. 2014). This reaction describes the composition of amino acid and sucrose exports from a mature Arabidopsis (*A. thaliana*) leaf, with output constrained to a 3:1 ratio for day:night.

Osmotic constraints

To calculate total osmotic concentration of the guard cell for a given stomatal aperture, we used the empirical relationship defined in the OnGuard model (Hills et al. 2012). The equations implemented here are:

$$Os_{ind} = \frac{RT}{4p} \cdot \left(\left(\frac{2 \cdot A \cdot (r+s) \cdot p}{RT} + C_{apo} + \frac{q}{RT} \right)^2 - \left(C_{apo} + \frac{q}{RT} \right)^2 \right)$$

$$Os_{total} = Os_{ind} \cdot N_{gcs}$$
$$q = (n - m) \cdot (s/r)$$
$$p = m/r$$

where A is guard cell aperture, r, s, n, and m are empirical parameters, R is the ideal gas constant (0.08205 $dm^3 \cdot atm \cdot K^{-1} \cdot mol^{-1}$), T is the temperature defined as 296.15 K in Horrer et al. (2016), C_{apo} is the sum of osmolyte concentrations in the apoplast, and Os_{ind} and Os_{total} are the total number of moles of osmolyte in individual guard cells and all the guard cells, respectively.

Then, to simulate turgor-pressure driven changes in guard cell volume, the model needed to generate the specified amount of total osmolyte from a range of specified metabolites and ions for the aperture values for differing phases. For this, we used the GrOE-FBA framework (Shameer et al. 2020). This framework imposes Os_{total} as a constraint during flux balance analysis (FBA) using "osmotic pseudo-metabolites" which are added to linker reactions for osmotic metabolites and ions in stoichiometric proportions. The linker reactions that were included in the osmolarity calculations are specified in Supplementary Table S1. Osmotic pseudo-metabolite fluxes were collected in an "aggregator reaction" with the constraint applied that the flux of the aggregator reaction in each temporal phase be equal to Os_{total}. The proportion of the cell that was vacuole was set at 0.751, with the rest of the cell defined as cytosol, according to Wang et al. (2017), and the aggregator reaction was constrained so that it consumed vacuolar and cytosolic osmotic pseudo-metabolites in this ratio, assuming equal osmotic concentration in the 2 compartments.

Accounting for maintenance costs (ATP and NADPH consumption)

Maintenance costs in a leaf are dependent on the incident light intensity and were implemented as described elsewhere (Töpfer et al. 2020). Moreover, to distribute maintenance costs between guard cells and mesophyll tissue, the light-independent portion of maintenance was distributed between the 2 cell types using a proxy based on their relative metabolic activities. More specifically, this relative metabolic activity was calculated based on the ratio of the total sum of metabolic and transport reaction fluxes for each cell type in the absence of any maintenance costs.

Obtaining the plasma membrane H^+-ATPase value using the OnGuard model

The model file "RCA5-wt-191120-wt", that was packaged with the Summer 2022 release of OnGuard 3 (Version 3.3.6.2) (Jezek et al. 2021) was modified by unticking the "CRR" box and then simulating 24 h. The average flux through the plasma membrane H^+-ATPase in the first half hour was then used as the upper bound for the plasma membrane H^+-ATPase.

FBA

FBA problems were set up and run using scripts in Python version 3.9 and the COBRApy package (Ebrahim et al. 2013) (version 0.27.0). The complete model with both cell types and all 4 temporal phases was solved as a single optimization problem using pFBA (Lewis et al. 2010). The primary optimization objective was to maximize phloem output, and the secondary objective was to minimize the sum of fluxes in the model. To account for the unequal duration of the 4 temporal phases in the sum of fluxes calculation, a phase-specific weighting was applied to each reaction flux, effectively multiplying the flux by the duration of the phase. Fluxes through the linker reactions were excluded from the weighting as these are not enzyme-catalyzed. Flux variability analysis was implemented as described elsewhere (Mahadevan and Schilling 2003).

Other analyses

The parameter combinations for the robustness analysis were generated using Latin hypercube sampling (Van Schepdael et al. 2016) and coded using the "lhs" function of the pyDOE package (version 0.3.8) (https://github.com/tisimst/pyDOE/). Linear regression and lasso linear regression were implemented using scikit learn (Garreta and Moncecchi 2013) (version 1.2.0). NBDev (https://github.com/fastai/nbdev) (version 2.3.7) was used for creating the Python package and documentation; matplotlib

(Hunter 2007) (version 3.6.0) and seaborn (Waskom 2021) (version 0.12.0) were used for plotting; escher (King et al. 2015) (version 1.7.3) was used for generating flux maps useful in analysis; and pandas (The pandas development team 2024) (version 1.5.0) and pandarallel (https://github.com/nalepae/pandarallel) (version 1.6.3) were used for data analysis. Color schemes were from Paul Tol (https://personal.sron.nl/~pault/).

Acknowledgments

The authors would like to thank Professor Mark Fricker, University of Oxford, for useful discussions.

Author contributions

N.S. performed research, contributed new computational tools, analyzed data, and co-wrote the paper. C.Y.M.C. analyzed the data and co-wrote the paper. S.S. contributed new computational tools. R.G. R. analyzed data and co-wrote the paper. L.J.S. designed the research, analyzed data, and co-wrote the paper. N.T. designed the research, analyzed data, and co-wrote the paper.

Supplementary data

The following materials are available in the online version of this article.

Supplementary Figure S1. Transfer of metabolites and ions.

Supplementary Figure S2. Transporters and channels in guard cells.

Supplementary Figure S3. Osmolyte concentrations and metabolic fluxes in the guard cell during opening in blue light without plasma membrane H+-ATPase constraint.

Supplementary Figure S4. Guard cell glycolytic flux in response to guard cell photosynthesis with respect to mesophyll photosynthesis.

Supplementary Table S1. List of linker reactions.

Supplementary Table S2. Parameter bounds for parameter sampling.

Supplementary Data Set 1. Guard cell metabolic model in SBML format.

Supplementary Data Set 2. Flux solutions of scenarios presented in this study.

Supplementary Data Set 3. List of reactions for energy and reducing power budget calculations.

Supplementary Data Set 4. Constraints used in parameter sampling.

Supplementary Data Set 5. Solution to parameter sampling in blue light.

Supplementary Data Set 6. Solution to parameter sampling in white light.

Funding

N.T. and C.Y.M.C. are funded by the Deutsche Forschungsgemeinschaft (DFG, the German Research Foundation) under Germany's Excellence Strategy (EXC-2048/1 – project ID 390686111).

Conflict of interest statement. None declared.

Data Availability

The code required to reproduce the results presented here is available at https://github.com/toepfer-lab/mmon-gcm, with documentation at https://toepfer-lab.github.io/mmon-gcm/.

References

Allaway WG, Setterfield G. Ultrastructural observations on guard cells of *Vicia faba* and *Allium porrum*. *Can J Bot*. 1972:50(6):1405–1413. https://doi.org/10.1139/b72-169

Amodeo G, Talbott LD, Zeiger E. Use of potassium and sucrose by onion guard cells during a daily cycle of osmoregulation. *Plant Cell Physiol*. 1996:37(5):575–579. https://doi.org/10.1093/oxfordjournals.pcp.a028983

Arnold A, Nikoloski Z. Bottom-up metabolic reconstruction of *Arabidopsis* and its application to determining the metabolic costs of enzyme production. *Plant Physiol*. 2014:165(3):1380–1391. https://doi.org/10.1104/pp.114.235358

Assmann SM, Jegla T. Guard cell sensory systems: recent insights on stomatal responses to light, abscisic acid, and CO_2. *Curr Opin Plant Biol*. 2016:33:157–167. https://doi.org/10.1016/j.pbi.2016.07.003

Assmann SM, Simoncini L, Schroeder JI. Blue light activates electrogenic ion pumping in guard cell protoplasts of *Vicia faba*. *Nature*. 1985:318(6043):285–287. https://doi.org/10.1038/318285a0

Azoulay-Shemer T, Palomares A, Bagheri A, Israelsson-Nordstrom M, Engineer CB, Bargmann BOR, Stephan AB, Schroeder JI. Guard cell photosynthesis is critical for stomatal turgor production, yet does not directly mediate CO_2- and ABA-induced stomatal closing. *Plant J*. 2015:83(4):567–581. https://doi.org/10.1111/tpj.12916

Blatt MR. Plant physiology: redefining the enigma of metabolism in stomatal movement. *Curr Biol*. 2016:26(3):R107–R109. https://doi.org/10.1016/j.cub.2015.12.025

Blatt MR, Jezek M, Lew VL, Hills A. What can mechanistic models tell us about guard cells, photosynthesis, and water use efficiency? *Trends Plant Sci*. 2022:27(2):166–179. https://doi.org/10.1016/j.tplants.2021.08.010

Chen Z-H, Hills A, Bätz U, Amtmann A, Lew VL, Blatt MR. Systems dynamic modeling of the stomatal guard cell predicts emergent behaviors in transport, signaling, and volume control. *Plant Physiol*. 2012:159(3):1235–1251. https://doi.org/10.1104/pp.112.197350

Cheung CYM, Poolman MG, Fell DA, Ratcliffe RG, Sweetlove LJ. A diel flux balance model captures interactions between light and dark metabolism during day–night cycles in C_3 and crassulacean acid metabolism leaves. *Plant Physiol*. 2014:165(2):917–929. https://doi.org/10.1104/pp.113.234468

Critchley JH, Zeeman SC, Takaha T, Smith AM, Smith SM. A critical role for disproportionating enzyme in starch breakdown is revealed by a knock-out mutation in Arabidopsis. *Plant J*. 2001:26(1):89–100. https://doi.org/10.1046/j.1365-313x.2001.01012.x

Daloso DM, Antunes WC, Pinheiro DP, Waquim JP, Araújo WL, Loureiro ME, Fernie AR, Williams TCR. Tobacco guard cells fix CO_2 by both Rubisco and PEPcase while sucrose acts as a substrate during light-induced stomatal opening. *Plant Cell Environ*. 2015:38(11):2353–2371. https://doi.org/10.1111/pce.12555

Daloso DM, Dos Anjos L, Fernie AR. Roles of sucrose in guard cell regulation. *New Phytol*. 2016a:211(3):809–818. https://doi.org/10.1111/nph.13950

Daloso DM, Williams TCR, Antunes WC, Pinheiro DP, Müller C, Loureiro ME, Fernie AR. Guard cell-specific upregulation of sucrose synthase 3 reveals that the role of sucrose in stomatal function is primarily energetic. *New Phytol*. 2016b:209(4):1470–1483. https://doi.org/10.1111/nph.13704

Daubermann AG, Lima VF, Erban A, Kopka J, Fernie AR, Schwarzländer M, dos Anjos L, Daloso DM. Novel guard cell sink characteristics revealed by a multi-species/cell-types meta-analysis of ^{13}C-labelling experiments. *Theor Exp Plant Physiol*. 2024:36(1):1–20. https://doi.org/10.1007/s40626-023-00299-9

Earles JM, Knipfer T, Tixier A, Orozco J, Reyes C, Zwieniecki MA, Brodersen CR, McElrone AJ. *In vivo* quantification of plant starch reserves at micrometer resolution using X-ray microCT imaging and machine learning. *New Phytol*. 2018:218(3):1269–1269. https://doi.org/10.1111/nph.15068

Ebrahim A, Lerman JA, Palsson BO, Hyduke DR. COBRApy: COnstraints-Based Reconstruction and Analysis for Python. *BMC Syst Biol*. 2013:7(1):74. https://doi.org/10.1186/1752-0509-7-74

Eisenach C, De Angeli A. Ion transport at the vacuole during stomatal movements. *Plant Physiol*. 2017:174(2):520–530. https://doi.org/10.1104/pp.17.00130

Engineer CB, Hashimoto-Sugimoto M, Negi J, Israelsson-Nordström M, Azoulay-Shemer T, Rappel W-J, Iba K, Schroeder JI. CO_2 sensing and CO_2 regulation of stomatal conductance: advances and open questions. *Trends Plant Sci*. 2016:21(1):16–30. https://doi.org/10.1016/j.tplants.2015.08.014

Feng L, Frommer WB. Structure and function of SemiSWEET and SWEET sugar transporters. *Trends Biochem Sci*. 2015:40(8):480–486. https://doi.org/10.1016/j.tibs.2015.05.005

Flütsch S, Horrer D, Santelia D. Starch biosynthesis in guard cells has features of both autotrophic and heterotrophic tissues. *Plant Physiol*. 2022:189(2):541–556. https://doi.org/10.1093/plphys/kiac087

Flütsch S, Wang Y, Takemiya A, Vialet-Chabrand SRM, Klejchová M, Nigro A, Hills A, Lawson T, Blatt MR, Santelia D. Guard cell starch degradation yields glucose for rapid stomatal opening in *Arabidopsis*. *Plant Cell*. 2020:32(7):2325–2344. https://doi.org/10.1105/tpc.18.00802

Fujiwara MT, Sanjaya A, Itoh RD. Leaf *Arabidopsis thaliana* epidermal guard cells: a model for studying chloroplast proliferation and partitioning in plants. *Front Plant Sci*. 2019:10:1403. https://doi.org/10.3389/fpls.2019.01403

Garreta R, Moncecchi G. *Learning scikit-learn: machine learning in Python*. Birmingham, UK: Packt Publishing Ltd; 2013.

Geilfus CM, Lan J, Carpentier S. Dawn regulates guard cell proteins in *Arabidopsis thaliana* that function in ATP production from fatty acid beta-oxidation. *Plant Mol Biol*. 2018:98(6):525–543. https://doi.org/10.1007/s11103-018-0794-x

Hedrich R, Raschke K, Stitt M. A role for fructose 2,6-bisphosphate in regulating carbohydrate metabolism in guard cells. *Plant Physiol*. 1985:79(4):977–982. https://doi.org/10.1104/pp.79.4.977

Hei S, Liu Z, Huang A, She X. The regulator of G-protein signalling protein mediates D-glucose-induced stomatal closure via triggering hydrogen peroxide and nitric oxide production in Arabidopsis. *Funct Plant Biol*. 2017:45(5):509–518. https://doi.org/10.1071/FP17180

Hills A, Chen Z-H, Amtmann A, Blatt MR, Lew VL. Onguard, a computational platform for quantitative kinetic modeling of guard cell physiology. *Plant Physiol*. 2012:159(3):1026–1042. https://doi.org/10.1104/pp.112.197244

Horrer D, Flütsch S, Pazmino D, Matthews JSA, Thalmann M, Nigro A, Leonhardt N, Lawson T, Santelia D. Blue light induces a distinct starch degradation pathway in guard cells for stomatal opening. *Curr Biol*. 2016:26(3):362–370. https://doi.org/10.1016/j.cub.2015.12.036

Hunter JD. Matplotlib: a 2D graphics environment. *Comput Sci Eng*. 2007:9(3):90–95. https://doi.org/10.1109/MCSE.2007.55

Inoue S-I, Kinoshita T. Blue light regulation of stomatal opening and the plasma membrane H^+-ATPase. *Plant Physiol*. 2017:174(2):531–538. https://doi.org/10.1104/pp.17.00166

Jezek M, Blatt MR. The membrane transport system of the guard cell and its integration for stomatal dynamics. *Plant Physiol*. 2017:174(2):487–519. https://doi.org/10.1104/pp.16.01949

Jezek M, Silva-Alvim FAL, Hills A, Donald N, Ishka MR, Shadbolt J, He B, Lawson T, Harper JF, Wang Y, et al. Guard cell endomembrane Ca^{2+}-ATPases underpin a 'carbon memory' of photosynthetic assimilation that impacts on water-use efficiency. *Nat Plants*. 2021:7(9):1301–1313. https://doi.org/10.1038/s41477-021-00966-2

Kelly G, Moshelion M, David-Schwartz R, Halperin O, Wallach R, Attia Z, Belausov E, Granot D. Hexokinase mediates stomatal closure. *Plant J*. 2013:75(6):977–988. https://doi.org/10.1111/tpj.12258

King ZA, Dräger A, Ebrahim A, Sonnenschein N, Lewis NE, Palsson BO. Escher: a web application for building, sharing, and embedding data-rich visualizations of biological pathways. *PLoS Comput Biol*. 2015:11(8):e1004321. https://doi.org/10.1371/journal.pcbi.1004321

Kinoshita T, Doi M, Suetsugu N, Kagawa T, Wada M, Shimazaki K-I. Phot1 and phot2 mediate blue light regulation of stomatal opening. *Nature*. 2001:414(6864):656–660. https://doi.org/10.1038/414656a

Knoblauch J, Waadt R, Cousins AB, Kunz H. Probing the *in situ* volumes of Arabidopsis leaf plastids using three-dimensional confocal and scanning electron microscopy. *Plant J*. 2023:117(2):332–341. https://doi.org/10.1111/tpj.16554

Korte P, Unzner A, Damm T, Berger S, Krischke M, Mueller MJ. High triacylglycerol turnover is required for efficient opening of stomata during heat stress in Arabidopsis. *Plant J*. 2023:115(1):81–96. https://doi.org/10.1111/tpj.16210

Kottapalli J, David-Schwartz R, Khamaisi B, Brandsma D, Lugassi N, Egbaria A, Kelly G, Granot D. Sucrose-induced stomatal closure is conserved across evolution. *PLoS One*. 2018:13(10):e0205359. https://doi.org/10.1371/journal.pone.0205359

Kruger NJ, Ratcliffe RG. Insights into plant metabolic networks from steady-state metabolic flux analysis. *Biochimie*. 2009:91(6):697–702. https://doi.org/10.1016/j.biochi.2009.01.004

Kwak JM, Murata Y, Baizabal-Aguirre VM, Merrill J, Wang M, Kemper A, Hawke SD, Tallman G, Schroeder JI. Dominant negative guard cell K^+ channel mutants reduce inward-rectifying K^+ currents and light-induced stomatal opening in *Arabidopsis*. *Plant Physiol*. 2001:127(2):473–485. https://doi.org/10.1104/pp.010428

Lawson T, Blatt MR. Stomatal size, speed, and responsiveness impact on photosynthesis and water use efficiency. *Plant Physiol*. 2014:164(4):1556–1570. https://doi.org/10.1104/pp.114.237107

Lawson T, Matthews J. Guard cell metabolism and stomatal function. *Annu Rev Plant Biol*. 2020:71(1):273–302. https://doi.org/10.1146/annurev-arplant-050718-100251

Lawson T, Oxborough K, Morison JIL, Baker NR. The responses of guard and mesophyll cell photosynthesis to CO_2, O_2, light, and water stress in a range of species are similar. *J Exp Bot*. 2003:54(388):1743–1752. https://doi.org/10.1093/jxb/erg186

Lawson T, Simkin AJ, Kelly G, Granot D. Mesophyll photosynthesis and guard cell metabolism impacts on stomatal behaviour. *New Phytol*. 2014:203(4):1064–1081. https://doi.org/10.1111/nph.12945

Lawson T, Vialet-Chabrand S. Speedy stomata, photosynthesis and plant water use efficiency. *New Phytol*. 2019:221(1):93–98. https://doi.org/10.1111/nph.15330

Lemonnier P, Lawson T. Calvin cycle and guard cell metabolism impact stomatal function. *Semin Cell Dev Biol*. 2024:155 Part:59–70. https://doi.org/10.1016/j.semcdb.2023.03.001

Lewis NE, Hixson KK, Conrad TM, Lerman JA, Charusanti P, Polpitiya AD, Adkins JN, Schramm G, Purvine SO, Lopez-Ferrer D, et al. Omic data from evolved *E. coli* are consistent with computed optimal growth from genome-scale models. *Mol Syst Biol*. 2010:6(1):390. https://doi.org/10.1038/msb.2010.47

Li Y, Xu S, Gao J, Pan S, Wang G. Glucose- and mannose-induced stomatal closure is mediated by ROS production, Ca^{2+} and water channel in *Vicia faba*. *Physiol Plant*. 2016:156(3):252–261. https://doi.org/10.1111/ppl.12353

Lim S-L, Flütsch S, Liu J, Distefano L, Santelia D, Lim BL. Arabidopsis guard cell chloroplasts import cytosolic ATP for starch turnover and stomatal opening. *Nat Commun*. 2022:13(1):652. https://doi.org/10.1038/s41467-022-28263-2

Lloyd FE. *The physiology of stomata*. Washington DC: Carnegie Institution of Washington; 1908.

MacRobbie EAC, Lettau J. Ion content and aperture in "isolated" guard cells of *Commelina communis* L. *J Membr Biol*. 1980:53(3):199–205. https://doi.org/10.1007/BF01868825

Mahadevan R, Schilling CH. The effects of alternate optimal solutions in constraint-based genome-scale metabolic models. *Metab Eng*. 2003:5(4):264–276. https://doi.org/10.1016/j.ymben.2003.09.002

McLachlan DH, Lan J, Geilfus CM, Dodd AN, Larson T, Baker A, Hõrak H, Kollist H, He Z, Graham I, et al. The breakdown of stored triacylglycerols is required during light-induced stomatal opening. *Curr Biol*. 2016:26(5):707–712. https://doi.org/10.1016/j.cub.2016.01.019

Medeiros DB, Perez Souza L, Antunes WC, Araújo WL, Daloso DM, Fernie AR. Sucrose breakdown within guard cells provides substrates for glycolysis and glutamine biosynthesis during light-induced stomatal opening. *Plant J*. 2018:94(4):583–594. https://doi.org/10.1111/tpj.13889

Outlaw WH. Current concepts on the role of potassium in stomatal movements. *Physiol Plant*. 1983:59(2):302–311. https://doi.org/10.1111/j.1399-3054.1983.tb00775.x

Outlaw WH. Critical examination of the quantitative evidence for and against photosynthetic CO_2 fixation by guard cells. *Physiol Plant*. 1989:77(2):275–281. https://doi.org/10.1111/j.1399-3054.1989.tb04981.x

Papanatsiou M, Amtmann A, Blatt MR. Stomatal clustering in Begonia associates with the kinetics of leaf gaseous exchange and influences water use efficiency. *J Exp Bot*. 2017:68(9):2309–2315. https://doi.org/10.1093/jxb/erx072

Piro L, Flütsch S, Santelia D. Arabidopsis sucrose synthase 3 (SUS3) regulates starch accumulation in guard cells at the end of day. *Plant Signal Behav*. 2023:18(1):e2171614. https://doi.org/10.1080/15592324.2023.2171614

Reckmann U, Scheibe R, Raschke K. Rubisco activity in guard cells compared with the solute requirement for stomatal opening. *Plant Physiol*. 1990:92(1):246–253. https://doi.org/10.1104/pp.92.1.246

Robaina-Estévez S, Daloso DM, Zhang Y, Fernie AR, Nikoloski Z. Resolving the central metabolism of Arabidopsis guard cells. *Sci Rep*. 2017:7(1):8307. https://doi.org/10.1038/s41598-017-07132-9

Santelia D, Lawson T. Rethinking guard cell metabolism. *Plant Physiol*. 2016:172(3):1371–1392. https://doi.org/10.1104/pp.16.00767

Santelia D, Lunn JE. Transitory starch metabolism in guard cells: unique features for a unique function. *Plant Physiol*. 2017:174(2):539–549. https://doi.org/10.1104/pp.17.00211

Scarth GW. Stomatal movement: its regulation and regulatory role a review. *Protoplasma*. 1927:2(1):498–511. https://doi.org/10.1007/BF01604752

Schnabl H, Raschke K. Potassium chloride as stomatal osmoticum in *Allium cepa* L., a species devoid of starch in guard cells. *Plant Physiol*. 1980:65(1):88–93. https://doi.org/10.1104/pp.65.1.88

Schwender J, König C, Klapperstück M, Heinzel N, Munz E, Hebbelmann I, Hay JO, Denolf P, De Bodt S, Redestig H, et al. Transcript abundance on its own cannot be used to infer fluxes in central metabolism. *Front Plant Sci*. 2014:5:668. https://doi.org/10.3389/fpls.2014.00668

Shameer S, Baghalian K, Cheung CYM, Ratcliffe RG, Sweetlove LJ. Computational analysis of the productivity potential of CAM. *Nat Plants*. 2018:4(3):165–171. https://doi.org/10.1038/s41477-018-0112-2

Shameer S, Ratcliffe RG, Sweetlove LJ. Leaf energy balance requires mitochondrial respiration and export of chloroplast NADPH in the light. *Plant Physiol*. 2019:180(4):1947–1961. https://doi.org/10.1104/pp.19.00624

Shameer S, Vallarino JG, Fernie AR, Ratcliffe RG, Sweetlove LJ. Flux balance analysis of metabolism during growth by osmotic cell expansion and its application to tomato fruits. *Plant J*. 2020:103(1):68–82. https://doi.org/10.1111/tpj.14707

Sperry JS, Venturas MD, Anderegg WRL, Mencuccini M, Mackay DS, Wang Y, Love DM. Predicting stomatal responses to the environment from the optimization of photosynthetic gain and hydraulic cost. *Plant Cell Environ*. 2017:40(6):816–830. https://doi.org/10.1111/pce.12852

Talbott LD, Zeiger E. Sugar and organic acid accumulation in guard cells of *Vicia faba* in response to red and blue light. *Plant Physiol*. 1993:102(4):1163–1169. https://doi.org/10.1104/pp.102.4.1163

Talbott LD, Zeiger E. Central roles for potassium and sucrose in guard-cell osmoregulation. *Plant Physiol*. 1996:111(4):1051–1057. https://doi.org/10.1104/pp.111.4.1051

Tan XLJ, Cheung CYM. A multiphase flux balance model reveals flexibility of central carbon metabolism in guard cells of C_3 plants. *Plant J*. 2020:104(6):1648–1656. https://doi.org/10.1111/tpj.15027

The pandas development team. pandas-dev/pandas: Pandas. Zenodo; 2024.

Töpfer N, Braam T, Shameer S, Ratcliffe RG, Sweetlove LJ. Alternative crassulacean acid metabolism modes provide environment-specific water-saving benefits in a leaf metabolic model. *Plant Cell*. 2020:32(12):3689–3705. https://doi.org/10.1105/tpc.20.00132

Van Schepdael A, Carlier A, Geris L. Sensitivity analysis by design of experiments. In: Geris L, Gomez-Cabrero D, editors. *Uncertainty in biology. Studies in mechanobiology, tissue engineering and biomaterials*. Vol. 17. Cham, Switzerland: Springer International Publishing; 2016. p. 327–366.

Vavasseur A, Raghavendra AS. Guard cell metabolism and CO_2 sensing. *New Phytol*. 2005:165(3):665–682. https://doi.org/10.1111/j.1469-8137.2004.01276.x

Wang Y, Hills A, Vialet-Chabrand S, Papanatsiou M, Griffiths H, Rogers S, Lawson T, Lew VL, Blatt MR. Unexpected connections between humidity and ion transport discovered using a model to bridge guard cell-to-leaf scales. *Plant Cell*. 2017:29(11):2921–2939. https://doi.org/10.1105/tpc.17.00694

Wang SW, Li Y, Zhang XL, Yang HQ, Han XF, Liu ZH, Shang ZL, Asano T, Yoshioka Y, Zhang CG, et al. Lacking chloroplasts in guard cells of crumpled leaf attenuates stomatal opening: both guard cell chloroplasts and mesophyll contribute to guard cell ATP levels. *Plant Cell Environ*. 2014:37(9):2201–2210. https://doi.org/10.1111/pce.12297

Waskom ML. seaborn: statistical data visualization. *J Open Source Softw*. 2021:6(60):3021. https://doi.org/10.21105/joss.03021

Woolfenden HC, Baillie AL, Gray JE, Hobbs JK, Morris RJ, Fleming AJ. Models and mechanisms of stomatal mechanics. *Trends Plant Sci*. 2018:23(9):822–832. https://doi.org/10.1016/j.tplants.2018.06.003

Wuyts N, Palauqui J-C, Conejero G, Verdeil J-L, Granier C, Massonnet C. High-contrast three-dimensional imaging of the Arabidopsis leaf enables the analysis of cell dimensions in the epidermis and mesophyll. *Plant Methods*. 2010:6(1):17. https://doi.org/10.1186/1746-4811-6-17

Zhang J, De-Oliveira-Ceciliato P, Takahashi Y, Schulze S, Dubeaux G, Hauser F, Azoulay-Shemer T, Tõldsepp K, Kollist H, Rappel W-J, et al. Insights into the molecular mechanisms of CO_2-mediated regulation of stomatal movements. *Curr Biol*. 2018:28(23):R1356–R1363. https://doi.org/10.1016/j.cub.2018.10.015

Zhu XG, Long SP, Ort DR. Improving photosynthetic efficiency for greater yield. *Annu Rev Plant Biol*. 2010:61(1):235–261. https://doi.org/10.1146/annurev-arplant-042809-112206